EVALUATION OF UNSATURATED FLOW IN FISSURED SEDIMENTS IN THE CHIHUAHUAN DESERT, TEXAS

by
Bridget R. Scanlon
Richard S. Goldsmith
Thomas C. Gustavson

Final Report

Prepared for

The National Low-Level Radioactive Waste Management Program,
U.S. Department of Energy, Assistant Secretary for Environmental Management
under the DOE Idaho Operations Office Contract No. DE-AC07-95ID13223

under Interagency Contract No. 94-0304

Bureau of Economic Geology
Noel Tyler, Director
The University of Texas at Austin
Austin, Texas 78713-8924

ABSTRACT

Localized flow in fissured sediments in arid settings has important implications for waste disposal in these regions. Fissures are surface features or gullies that are underlain by partially open or sediment-filled fractures. The objectives of this study were to compare unsaturated flow beneath different fissures, investigate the vertical and lateral extent of increased flow associated with fissured sediments, and examine different techniques for evaluating flow in fissured zones. Boreholes were drilled directly beneath four fissures and at distances of 10 and 50 m from the fissures. Sediment samples were analyzed for hydraulic parameters such as water content and water potential and environmental tracers such as Cl, $^{36}Cl/Cl$, ^{3}H, ^{2}H, and ^{18}O. A trench was dug beneath one fissure for detailed sampling. Electromagnetic induction was used to measure apparent electrical conductivity in transects perpendicular to the fissures.

Unsaturated flow is relatively high beneath fissures, as evidenced by higher water potentials and lower chloride concentrations there than in surrounding sediments. The lateral extent of high water flux was restricted to the zone directly beneath one fissure but extended to profiles 10 m from two other fissures. The profiles 50 m distant from all fissures had low water fluxes, as indicated by low water potentials and high maximum chloride concentrations. The vertical extent of high water fluxes was restricted to the upper 10 to 20 m, as shown by water potential and chloride fronts within the upper 10 m zone beneath one fissure and by chloride fronts in the upper 20 m zone beneath and 10 m distant from another fissure. Additional evidence for localized water flux was provided by high tritium levels, less-enriched ^{2}H and ^{18}O, and higher plant water potentials in fissured sediments than in nonfissured sediments. Apparent electrical conductivity was higher in two of the four fissures. Multiple independent lines of evidence indicate that subsurface water fluxes are higher at shallow depths beneath fissures; however, the various techniques differ in their effectiveness in delineating higher water fluxes beneath fissures. Multiple profiles drilled in one

fissure indicate that there is large variability in flow along this fissure that is attributed to topographic variations and degree of ponding.

INTRODUCTION

Surface fissures have been found in semiarid and arid regions throughout the western United States from southern California to western Texas and as far north as Idaho (Baumgardner and Scanlon, 1992). Linear systems of fissures may be as much as 15 km long (Slaff, 1989). Individual fissures as wide as 15 m and fractures as deep as 25 m have been found (Boling, 1986; Slaff, 1989).

The term *fissure* refers to the alignment of discontinuous surface-collapse structures, or gullies; the underlying extensional feature, termed a *fracture*, is filled with sediment. Fissures commonly form in sediments near margins of alluvial valleys. They are generally oriented parallel or subparallel to the long axis of the host valley and approximately perpendicular to tributary drainage. Because of their orientation, they intercept runoff, which erodes the fissures into wide gullies. The increased runoff into fissured sediments results in higher water content and more vegetation in these zones.

Many fissures have formed where sediment compaction and land subsidence have resulted from groundwater withdrawal, particularly in Arizona (Schumann and others, 1986). However, some fissures have formed in areas where groundwater pumping has been minimal or before extensive groundwater pumping began (Slaff, 1989; Robinson and Peterson, 1962). Baumgardner and Scanlon (1992) suggested that the model for fissure development proposed by Larson and Pewe (1986) should be applicable to fissures in the study area. According to this model, the initial feature is a fracture that forms in the shallow subsurface and allows water to move down from the surface. Water movement leads to erosion of the fracture and creates soil pipes. Eventually the sediments overlying the pipes collapse, which results in surface gullies that concentrate runoff. The gullies eventually connect, and the final phase is marked by plugging of the soil pipes and filling of the fissure with sediment.

Previous Studies

Geomorphic and hydrologic studies conducted in the Hueco Bolson fissure are described in Baumgardner and Scanlon (1992) and Scanlon (1992b). Hydraulic studies and environmental and applied tracer studies were conducted to evaluate unsaturated flow in the fissured sediments. Collection of sediment samples was restricted to a profile beneath the fissure and to two profiles at distances of 3 m and 6 m from the fissure. The maximum borehole depth was 9 m. These samples were analyzed for texture, water content, water potential, and chloride concentration. In addition, a tracer experiment was conducted in a trench dug 4 m deep to compare flow and transport in the fracture fill with that in surrounding sediments. The results of these studies showed that subsurface water fluxes were higher beneath the fissure, as indicated both by higher water potentials than in surrounding geomorphic settings and by lower maximum chloride concentrations (80 to 105 g m^{-3}, compared with 2,000 to 6,000 g m^{-3}). The applied tracer experiment showed higher water and solute transport in the fracture-fill sediment than in adjacent sediments. The fissure was marked by a lineation of honey mesquite (*Prosopsis glandulosa*). Roots of these plants extended to a depth of at least 6 m in the fracture-fill sediments, which suggests that plants may play an important part in removing water from these areas by evapotranspiration.

Objectives

The objectives of this study were to compare unsaturated flow beneath different fissures, to determine the vertical and lateral extent of increased flow in fissured sediments, and to evaluate different techniques of estimating unsaturated flow. Fissures evaluated in this study included the Hueco Bolson fissure that was previously studied (Scanlon, 1992b) and three additional fissures. The vertical extent of unsaturated flow was evaluated by drilling and sampling boreholes to a maximum depth of 31 m; in the previous investigation of the Hueco Bolson fissure, the maximum borehole depth was 9 m. To evaluate the lateral extent of increased flow associated with fissures, boreholes for this study were drilled at distances of 10 and 50 m from each fissure; the previous

study included only boreholes at distances of 3 and 6 m. A large trench was excavated beneath one fissure for detailed sampling. Previous studies used hydraulic and environmental tracer techniques to evaluate flow in fissured sediments (Baumgardner and Scanlon, 1992). In this study, the number of techniques was greatly increased. In previous studies, chloride was the only environmental tracer used; in this study, chloride, chlorine-36, tritium, and stable isotopes of oxygen and hydrogen were also used. This study also evaluated noninvasive techniques such as electromagnetic induction and plant water potentials. The following provides a brief description of the theoretical basis for the techniques used.

Hydraulic Parameters

Hydraulic data included measurement of water content and water potential on sediment samples collected from boreholes drilled in and adjacent to the fissures. Water content is discontinuous across different sediment types; therefore, variations in water content measured at one time cannot be used to evaluate the direction of water movement. In contrast, water potential is continuous across different textural interfaces under steady flow conditions, and water potential gradients can be used to assess the direction of water movement. Predawn plant water potentials are generally considered to indicate water potential in unsaturated sediments and should provide a noninvasive technique of estimating unsaturated flow. Because vegetation, particularly mesquite, is much more dense along fissures than in adjacent nonfissured sediments, vegetation probably plays an important role in controlling water flux in fissured sediments. Previous studies showed that water potentials in the unsaturated zone were much higher in fissured sediments than in adjacent nonfissured sediments (Scanlon, 1992b); therefore, predawn plant water potentials in fissured zones should be higher than those in adjacent nonfissured sediments.

Electromagnetic Induction

Electromagnetic induction provides a noninvasive technique for evaluating apparent electrical conductivity of the sediments. Fractures and soil pipes with associated high water flux may exist in the subsurface for a long time with little surface expression; therefore, noninvasive techniques may be particularly useful for delineating these zones prior to surface collapse and gully formation. Previous studies of fissured sediments showed that pore-water chloride was flushed out in fissured sediments. Zones of low pore-water chloride concentration are particularly characteristic of fissured sediments, and it was thought that they should result in low apparent electrical conductivity that could be detected with electromagnetic induction.

Environmental Tracers

Environmental tracers are being used extensively to quantify water fluxes in the unsaturated zone. Chloride concentrations in pore water have been widely used to evaluate water fluxes in arid and semiarid systems (Allison and Hughes, 1978; Edmunds and Walton, 1980; Phillips, 1994). Chloride concentrations in pore water in the unsaturated zone increase through the root zone as a result of evapotranspiration because chloride is essentially nonvolatile and plant uptake is negligible. Low chloride concentrations reflect high water fluxes that either minimize accumulation of chloride or flush out previously accumulated chloride. High chloride concentrations indicate low water flux.

The subsurface distribution of bomb-pulse tracers such as chlorine-36 and tritium provides information on water movement during the past 30 to 40 yr. Chlorine-36 (half-life 301,000 yr) was enriched by neutron activation of chlorine-35 in sea water by nuclear weapons tests conducted between 1952 and 1958, exceeding natural production by up to three orders of magnitude and peaking in 1955 (Bentley et al., 1986). Chlorine-36 is a tracer of liquid flow because chlorine-36 entered the hydrologic cycle as chloride, which is essentially nonvolatile. Tritium (half-life 12.4 yr) concentrations increased from 10 to $\geq$ 2,000 TU during atmospheric nuclear testing that began in

1952 and peaked in 1963–1964. Tritiated water can exist in both liquid and vapor phases; therefore, tritium is a tracer for liquid and vapor water movement.

Site Description

Fissures examined in this study are located in intermontane basins within the Basin and Range physiographic province in Trans-Pecos Texas (fig. 1). Studies were conducted in the Hueco Bolson, Red Light Bolson, Eagle Flat, and Ryan Flat fissures. All fissures are found in alluvial fill sediments. Depth to groundwater ranges from 85 m (Ryan Flat fissure) to 215 m (Eagle Flat fissure).

Three of the four studied fissures are described in detail in Baumgardner and Scanlon (1992), and the fourth fissure (Eagle Flat) is described in Jackson et al. (1993). Therefore, only brief descriptions are provided here. The names of some of the fissures have been changed from the original reports; for example, Hoover fissure in Jackson et al. (1993) corresponds to Eagle Flat fissure, and Quitman Canyon fissure in Baumgardner and Scanlon (1992) is now called Red Light Bolson fissure. Width-to-depth (width/depth) ratios of surface gullies of fissures provide some indication of the maturity of the fissures and range from 0.1 to 28; however, most are ≤ 5. Very low width/depth ratios are indicative of young fissures, whereas those with high width/depth ratios are probably filling and widening and are relatively mature.

The three fissures mapped in the Hueco Bolson ranged from 21 to 140 m long. These fissures are in fairly coarse textured sediments. Studies were conducted in the 140-m-long fissure, which had width/depth ratios that ranged from 0.2 to 2. This fissure is marked by honey mesquite trees (*Prosopsis glandulosa*). The surface-collapse features are separated by bridges of sediment that overlie soil pipes. Spacing between collapsed sections is generally 1 to 3 m. Trenches revealed subsurface fractures that extend to a depth of at least 6.2 m (fig. 2a). The fracture ranges in width from 65 mm at 3.8 m depth to 25 mm at 5.6 m depth and is filled with sediment. The fissure is not visible on aerial photographs because of large creosote bushes (*Larrea tridentata*) adjacent to the fissured sediments.

The fissure studied in Red Light Bolson lies at the toe of a dissected alluvial fan. The fissure trends N10°–25°W, parallel to topographic contours and to the valley axis. Fissures in this area were up to 4.2 km long on aerial photographs taken in 1957. The northwest-trending fissures are perpendicular to the ephemeral stream channels and intercept runoff. Mesquite trees are denser in the vicinity of the fissure. These fissures have filled with sediment and have width/depth ratios up to 5. Another section of the Red Light Bolson fissures showed evidence of recent collapse and had steep gullies (3.6 m deep and 0.8 m wide). Calcic soil development is much greater in this section of the fissure and maintains the open gullies.

The northwest Eagle Flat fissure examined in this study differs in location from the Eagle Flat fissures described in Baumgardner and Scanlon (1992), which are located in the Booth property. This fissure is 640 m long and is clearly delineated on aerial photographs (fig. 3) and on the ground by mesquite trees. It consists of depressions that average 20 m long, 1 m wide, and 0.3 m deep. Trenches dug to a maximum depth of 6 m showed a modern calcic soil and three buried calcic horizons (fig. 2b). The fissure or gully is underlain by a tension fracture that is most obvious at depths of 2 m or more. At shallower depths, the fracture is not as obvious because of slumping of sediments. The width of the eroded fracture is ~ 0.2 m in the depth zone from 2 to 6 m. At ~ 3.5 m depth the fracture bifurcates, and one of the bifurcations is only 0.04 m wide. The maximum vertical extent of the fracture is unknown because the trench did not reach the base of the fracture. The fracture fill sediments are slightly coarser grained than the surrounding material. The fissure formed as a result of near-surface tensional stresses.

The Ryan Flat fissure formed in 1990. This fissure was 2.2 m deep and 0.7 m wide at its deepest part, which results in a width/depth ratio of 0.1 and is consistent with the young age of the fissure. Traces of an old fissure near the 1990 fissure are indicated by elongated shallow swales and aligned mesquite bushes adjacent and parallel to the new fissure. This suggests that the new fissure is opening where an older fissure existed. Surface collapse of sediment was also reported in 1935, and the recent changes probably mark the time of a rainfall event that produced erosion and collapse of soils along a preexisting fracture.

METHODS

Sediment samples were collected for laboratory measurement of physical and chemical parameters from 18 boreholes drilled in and adjacent to 4 fissures (fig. 1, table 1). Borehole depths ranged from 8.7 m (RLB 50m) to 30.6 m (EFF36 10m). Sediment samples were also collected from a trench excavated in a series of benches (~1.3 m high) that were progressively narrower with depth beneath the Eagle Flat fissure (fig. 2b). A grid was placed on the trench face, and samples were collected at approximately 0.3 m intervals in a 4.2-m-wide section at the surface that was progressively narrower at depth (fig. 2b). A total of 124 samples were collected for water content and chloride analyses, and 7 samples were taken in and adjacent to the fracture fill for water potential analysis. The samples were collected immediately after each bench was cleared. Additional material was removed from the trench face with a shovel and knife prior to sampling.

Particle-size analyses were conducted on sediment samples by sieving the ≥ 0.05 mm fraction to determine the percent sand and by conducting hydrometer or pipette analysis of the < 0.05 mm fraction to determine the percent silt and clay (Gee and Bauder, 1986). Carbonate was not dissolved in these samples because some of the rock fragments were carbonate. Sediment samples that contained ≥ 5 % gravel were classified according to Folk (1974), and those that lacked gravel were classified according to the U.S. Department of Agriculture (1975). Gravimetric water content was measured by oven drying the sediment samples at 105°C for 24 hr. Neutron-probe access tubes were installed beneath the Eagle Flat fissure and 10 m distant from the fissure to a depth of 8.4 m to monitor temporal variations in water content (fig. 1). Water content was monitored with a neutron moisture probe (Model 503DR; Campbell Pacific Nuclear Corporation, Martinez, CA).

Water potential was measured in the laboratory using a thermocouple psychrometer with a sample changer (model SC 10A; Decagon Devices, Inc., Pullman, WA). The Decagon SC 10A was calibrated using NaCl solutions that ranged in concentration from 0.05 molal to saturated and corresponded to water potentials of -0.2 to -38 MPa at 20°C (Lang, 1967). The standard error of estimate for the SC 10A thermocouple psychrometer (based on analysis of 20 calibration solutions)

was 0.06 MPa. The osmotic component of water potential was calculated from pore-water chloride concentrations according to the van't Hoff equation (Campbell, 1985; Scanlon, 1994). Samples with high water potentials collected from a trench beneath the Eagle Flat fissure were analyzed using both the Decagon SC 10A sample changer and the filter paper method (ASTM D-5298-92, 1992). The filter paper was placed in the center of the sediment samples in glass containers and was allowed to equilibrate for two weeks. After equilibration, the mass of the filter paper was determined and was related to the matric potential through calibration curves developed by Greacen et al. (1987).

Predawn plant water potentials were measured in and adjacent to the fissures using a portable pressure chamber apparatus (Plant Moisture Stress, Inc., Corvallis, OR) by removing at least two randomly chosen stems containing leaves from each plant and immediately measuring their water potential. The stems were wrapped in plastic to minimize sample drying prior to measurement and to prevent sample burning by nitrogen in the pressure chamber. Stems were collected from mesquite plants within and adjacent to fissures except at the Hueco Bolson fissure, where creosote bushes were sampled because mesquite trees were not found outside the fissure. Plant water potentials were measured periodically for 1 year. Samples were not collected in March because the plants were defoliated and dormant.

To determine chloride content, double-deionized water was added in a 3:1 ratio to the dried sediment samples that had previously been analyzed for water content. Samples were agitated on a reciprocal shaker table for 4 hr. The supernatant was filtered through 0.45 μm filters. Chloride was then analyzed by ion chromatography or by potentiometric titration.

Laboratory preparation of chloride samples for ^{36}Cl analysis followed procedures outlined in Scanlon (1992a). The $^{36}Cl/Cl$ ratios were measured by accelerator mass spectrometry at Lawrence Livermore National Laboratory. To evaluate chemical contamination during sample preparation, reagent grade NaCl was subjected to the same purification procedure as the sediment samples. Uncertainties were calculated following Elmore et al. (1984) and are reported as one standard deviation.

Water for tritium analysis was extracted from sediment samples by azeotropic distillation with toluene (Allison et al., 1985). After distillation the water samples were purified of toluene by heating in paraffin wax. Tritium was analyzed by the University of Arizona Tritium Laboratory using enrichment factors that ranged from 2 to 9 depending on the amount of water available. The detection limit for enriched tritium analyses was 0.7 TU and the standard errors were ≤ 1.4 TU. Stable-isotope analyses of oxygen and hydrogen were conducted by Desert Research Institute according to procedures outlined in Ingraham and Shadel (1992).

Two different Geonics instruments (EM31 and EM38; Geonics Inc., Mississauga, Canada) were used to measure apparent electrical conductivity of the subsurface along transects perpendicular to the trend of the fissures for distances of up to 100 m on either side. The theoretical basis for these measurements is described in McNeill (1992). The intercoil spacing in the EM38 is 1.0 m, whereas that in the EM31 is 3.7 m. The difference in intercoil spacing results in different exploration depths for these instruments: 0.75 m for the EM38 and 3.0 m for the EM31 when the instruments are operated in the horizontal dipole mode (both coils vertically on the ground), 1.5 m for the EM38 and 6 m for the EM31 when the instruments are operated in the vertical dipole mode (both coils horizontally on the ground). In this study, both instruments were operated in the horizontal and vertical dipole modes to evaluate changes in conductivity with depth.

RESULTS

Texture and Water Content

The texture of the sediments that host the fissures is variable (table 2). Sediment texture in and adjacent to the Hueco Bolson and Red Light Bolson fissures is much coarser grained than that in and adjacent to the Eagle Flat and Ryan Flat fissures. This reflects the regional geologic setting of these fissures. Sediment samples beneath and adjacent to the Hueco Bolson fissure have mean sand contents that range from 44 to 55% in the different profiles (tables 2 and 3). Textures in the Red Light Bolson fissure are generally coarse grained (mean sand content 36 to 41%). In contrast,

textures beneath the Eagle Flat fissure are predominantly silt (mean silt content 22 to 40%) or clay (mean clay content 24 to 45%), and those beneath the Ryan Flat fissure are predominantly clay (mean clay content 37 to 41%) with local zones of gravelly material (tables 2 and 3).

Water content was only monitored in and adjacent to the Eagle Flat fissure to assess penetration of water after rainfall events (fig. 4). The monitoring data showed water penetration to 1.2 m depth beneath the fissure after 131 mm of rain fell in July 1993 (38 mm in one day); however, the infiltrated water was removed from the subsurface by evapotranspiration in ~ 3 months (fig. 4a). These data show how effectively the mesquite bushes along the fissure remove infiltrated water. Water penetrated to depths ≥8.4 m beneath the fissure (EFF55NP, fig. 4b; 8.4 m is the depth of the access tube) after 116 mm of rain fell in September 1995. Ponding probably occurred after intense rain in the fissure because 69 mm of rain fell in one day (September 15). Maximum water content increases ranged from 0.15 to 0.28 $m^3\ m^{-3}$ beneath the fissure. Although only 20 mm of rain fell from October 1995 through April 1996, monitored water contents remained elevated (fig. 4b). The zone of infiltration beneath the fissure was localized, as evidenced by the absence of variations in water content in a neutron probe access tube 10 m from the fissure (EFF56NP; fig. 4c).

The deep penetration of water to ≥8.4 m beneath the fissure after the September 1995 rainfall contrasts with the shallow penetration of water after the July 1993 rainfall. A ponding test was conducted (Feb. 19, 1997) with bromide and FD&C blue dye to evaluate the nature of water movement adjacent to the neutron-probe access tube. A 4 m^2 area was ponded to a depth of 0.15 m for 8 hr. Two boreholes were drilled in the ponded area (February 25 through February 28, 1997). Sediment samples collected in boreholes drilled both immediately adjacent to (EFF122) and 0.6 m from (EFF121) the neutron-probe access tube showed leaching of chloride and high bromide concentrations in the upper meter beneath the ponded surface (fig. 5c and d; table 4). High chloride concentrations at depths of 1.7 to 2.6 m (EFF122, 4,600 to 4,800 g m^{-3}) suggest that water is not moving uniformly downward diluting chloride concentrations. Chloride concentrations at depths ≥ ~10 m suggest very little water movement below the maximum depth of the access tube (8.4 m).

Measured water potentials decreased markedly at depths ≥ 10 m (table 4, fig. 5b), which is consistent with the chloride data (fig. 5c). Trenching revealed much corrosion of the neutron-probe access tube. Wet clay sediments immediately adjacent to the access tube may reflect annular flow. Although annular flow is likely, the annular space may have been sealed after the September 1995 rainfall, which would have precluded further annular flow during the ponding test.

The monitoring data show how dynamic the unsaturated flow processes are beneath the fissures. Water content was also measured in sediment samples from boreholes in different locations in the Eagle Flat fissure (fig. 1). The boreholes were sampled at different times (table 1), which may affect interborehole comparisons. In all cases, water content in profiles in the Eagle Flat fissure was higher than that in profiles 10 m from the fissure, at least in the upper 5 to 10 m (fig. 6d, g, j, and m). These differences in water content cannot be attributed to textural differences and are related to higher water fluxes beneath the fissure as seen from the neutron-probe monitoring data. Water content differences were greatest between EFF120 0m and EFF119 10 m (fig. 6m), which are located in the central portion of the fissure where there is a large gully.

There was no systematic variation in water content in profiles beneath and adjacent to the other fissures (figs. 6a and 7a and d; tables 2, 3, and 5). Spatial variations in water content were generally related to variations in sediment texture. Water content was generally negatively correlated with percent sand and gravel and was positively correlated with percent clay (table 3). The lack of variations in water content between profiles in three of the four fissures relative to profiles adjacent to these fissures may be related in part to the sampling time. Boreholes in and adjacent to the Hueco Bolson, Red Light Bolson, and Ryan Flat fissures were drilled in 1994, when precipitation was much less than the long-term mean precipitation. Precipitation in 1994 was only 33% of the long-term mean (280 mm) in the Hueco Bolson, 44% of the long-term mean (320 mm) in Sierra Blanca (adjacent to Eagle Flat fissure), and 40% of the long-term mean (384 mm) in Valentine (adjacent to the Ryan Flat fissure).

Unsaturated-Zone Water Potentials

Water potentials (sum of matric and osmotic potential) in the unsaturated zone were generally higher in profiles beneath the fissures than in profiles adjacent to the fissures in the upper 6 to 15 m (figs. 6b, e, h, k, and n; 7b and e; table 6). Water potentials were as high as -0.2 MPa beneath the Hueco Bolson, Eagle Flat, and Ryan Flat fissures. These water potentials may not be highly accurate because of the standard error of the laboratory-measured water potentials with the Decagon SC 10A thermocouple psychrometer in this range (~±0.06 MPa). Water potentials measured with the filter paper method for samples collected in the trench beneath the Eagle Flat fissure agreed well with those measured with the Decagon thermocouple psychrometer for the range between -0.20 and -0.16 MPa (table 7); however, the agreement was poor in the wetter range, where some of the water potentials measured by the Decagon thermocouple psychrometer were positive (table 7). Water potentials were higher in the fracture-fill material (-0.02 to -0.01 MPa) than in the adjacent sediments (-0.20 to -0.16 MPa). The Eagle Flat fissure differed from the other fissures in that water potentials decreased below the zone of high water potentials (fig. 6e, h, k, and n), whereas in all the other profiles water potentials remained high at depth (figs. 6b and 7b and e). This reduction in water potential at depth in the Eagle Flat fissure marked the wetting front. This front was most clearly seen in EFF35 0m (fig. 6e); it was more diffuse in the other three profiles (fig. 6h, k, and n). In profile EFF35 0m, water potentials decreased from -0.8 MPa at 9.1 m to -5.0 MPa at 12.8 m depth (table 6). Below 13 m, water potentials in EFF35 0m were similar to those in the profile 10 m from the fissure (EFF 36 10m). Water potentials in the other profiles beneath Eagle Flat fissure (EFF88 0m, EFF92 0m, and EFF120 0m) were generally lower than those in EFF35 0m.

The static equilibrium line plotted on all graphs (figs. 6b, e, h, k, n, 7b, e) represents the matric potential that would exist if the unsaturated zone were in static equilibrium with the water table, a no-flow line where matric and gravity forces are balanced. Matric potentials that plot to the right of the static equilibrium line indicate downward flow under steady flow conditions, whereas

matric potentials that plot to the left of the static equilibrium line indicate upward flow under steady flow conditions. The osmotic component of water potential was negligible beneath the fissures because of low chloride concentrations; therefore, water and matric potentials are equivalent (table 6). The zone of high water potentials beneath the fissures plots to the right of the equilibrium line, indicating downward flow, except in the Red Light Bolson fissure (fig. 7b). Low water potentials in the shallow subsurface zone in some profiles beneath the fissure also plot to the left of the equilibrium line, indicating near-surface evapotranspiration (figs. 6b, h, and k; 7e). The water potential gradient also provides information on the direction of water flow. Zero water potential gradients indicate gravity drainage, as seen in EFF35 0m (fig. 6e).

Water potentials in profiles adjacent to the fissures were low at the surface ($\geq$ -27.4 MPa) and generally increased with depth, which indicates an upward driving force for water movement (fig. 6b, e, k, and n; 7b and e). These profiles also plot to the left of the equilibrium line, which further indicates upward flow under steady flow conditions. The low precipitation in 1994, when many of the profiles were drilled (table 1), may have affected the difference in water potential between fissured and nonfissured profiles.

Plant Water Potential

Predawn water potentials in plants were significantly higher in the Hueco Bolson ($\alpha = 0.05$), Eagle Flat ($\alpha = 0.06$), and Ryan Flat ($\alpha = 0.05$) fissures than adjacent to these fissures (fig. 8a, b, and d; table 8).The difference in predawn plant water potentials was most obvious in the Ryan Flat fissure, a very active fissure. The average water potential in plants at this fissure was -1.6 MPa, whereas that in plants adjacent to the fissure was -3.4 MPa (tables 2 and 8). Mean plant water potentials ranged from -2.7 MPa in the Hueco Bolson fissure to -4.8 MPa 50 m from the fissure (table 2). The difference in mean plant water potentials between the Eagle Flat fissure (-1.7 MPa) and 50 m from the fissure (-2.0 MPa) was much less than that in the other settings. There was no systematic difference in predawn plant water potentials in the Red Light Bolson fissure relative to

the adjacent area (fig. 8c). The monitoring interval was not sufficient to evaluate seasonal or shorter-term variations in plant water potentials.

Environmental Tracers

Meteoric Chloride

Chloride concentrations are expressed as g Cl m^{-3} pore water (equivalent to mg Cl L^{-1} pore water). In general, chloride concentrations were lower in profiles beneath fissures than in profiles adjacent to fissures (figs. 6c, f, i, l, o; 7c and f; table 5). Previous studies of the Hueco Bolson fissure showed low chloride concentrations (≤ 110 g m^{-3}) in the upper 10 m in the profile immediately beneath the fissure and in profiles at 3 and 6 m from the fissure (Scanlon, 1992b). In this study, profiles beneath the Hueco Bolson fissure and 10 m from the fissure had low chloride concentrations (mean 20 g m^{-3}, upper 14 m, beneath fissure, mean 48 g m^{-3}, upper 12 m, 10 m from fissure), whereas chloride concentrations in the profile 50 m distant from the fissure were high (mean 1,623 g m^{-3}, maximum 5,437 g m^{-3}, 3.1 m depth, fig. 6c). Chloride concentrations beneath the fissure increased from 2.5 g m^{-3} at 14.1 m depth to 1,300 g m^{-3} at the 21.1 m depth that probably marked the extent of flushing. The profile 10 m from the Hueco Bolson fissure also had a chloride front that was sharper than that beneath the fissure and also shallower (2.9 g m^{-3} at 11.0 m to 1,792 g m^{-3} at 15.2 m).

Low chloride concentrations were restricted to the zone immediately beneath the Eagle Flat fissure; the profile 10 m from the fissure had high concentrations (fig. 6f, i, l, and o). Chloride concentrations were low (≤ 196 g m^{-3}) in the upper 9 m of the profile EFF35 0m but increased sharply to 5,205 g m^{-3} within a 2 m depth interval (fig. 6f). The solute front in EFF120 0m was much more diffuse; chloride concentrations increased from < 158 g m^{-3} in the upper 8.3 m to 4,008 g m^{-3} at 16.7 m depth. The degree and vertical extent of chloride leaching were similar in EFF35 and EFF120 (fig. 6f and o), but both were much less in EFF88 and EFF92 (fig. 6i and l). Chloride concentrations at depth beneath the Eagle Flat fissure were similar to those in the profile

10 m from the fissure (fig. 6f, i, l, and o). Chloride concentrations adjacent to the Eagle Flat fissure were highest at or near the surface and generally decreased with depth. The solute front in EFF35 0m correlates with a slight reduction in chloride in the profile 10 m distant from 4,746 to 3,405 g m^{-3}, which may reflect lateral flow. Sharp changes in chloride concentrations are also found in EFF59 10 m (reduction from 5,510 g m^{-3} at 14.2 m depth to 3,286 g m^{-3} at 15.8 m depth and increase to 8,804 g m^{-3} at 17.4 m depth, fig. 6i).

Detailed sampling in a trench in the Eagle Flat fissure (figs. 2b and 9, table 9) showed that the horizontal extent of chloride flushing was much more restricted than the 10 m indicated by the borehole data. The sampling grid was centered on the surface expression of the fissure; however, the subsurface fracture was offset to the south of the surface fissure. High chloride concentrations were found about 1.2 m north of the underlying fracture at depths of 2 to 3 m and generally 1.8 m or more south of the fracture. The shape of the trench precluded sampling along a uniform grid.

Chloride concentrations in the profile beneath the Red Light Bolson fissure were low throughout ($\leq$ 97 g m^{-3}) with the exception of a local higher zone (151 to 844 g m^{-3}) from 4.5 to 6 m depth (fig. 7c; table 5). The chloride profile 50 m distant from the fissure had high chloride concentrations that ranged from 2,991 g m^{-3} at 0.76 m to 1,141 g m^{-3} at 8.2 m depth. Chloride concentrations were fairly low ($\leq$ 292 g m^{-3}) throughout the profile in the Ryan Flat fissure and increased gradually away from the fissure (fig. 7f, table 5). Maximum concentrations were 2,980 g m^{-3} at 1.3 m in the profile 10 m from the fissure and 757 at 1.7 m in the profile 50 m from the fissure. At depths $\geq$ 10 m all three profiles had similar chloride concentrations (8 to 297 g m^{-3}).

Isotopes

It was difficult to collect sufficient chloride for ^{36}Cl analysis beneath fissures. Where sufficient chloride was available, $^{36}Cl/Cl$ ratios were low (383×10^{-15} in EFF 92 to 713×10^{-15} in RLB 0m; fig. 10, table 10) and do not indicate significant contribution from the bomb pulse. Previous studies in an ephemeral stream setting at the Hueco Bolson study area included analysis of the distribution of bomb-pulse ^{36}Cl and showed that the $^{36}Cl/Cl$ ratios typical of the bomb pulse

reached a maximum value of $6{,}560 \times 10^{-15}$ (Scanlon, 1992a), and prebomb $^{36}Cl/Cl$ ratios were approximately 460×10^{-15}.

Tritium concentrations were high in all profiles analyzed for tritium beneath and adjacent to fissures (fig. 10, table 10). There was no systematic variation in tritium concentrations with depth. Tritium concentrations were high in profiles beneath the Eagle Flat fissure (fig. 10c) and beneath and 10 m from the Hueco Bolson fissure (fig. 10a and b), which is consistent with chloride being flushed out in these profiles also. Tritium concentrations were also high in the profile 10 m from the Eagle Flat fissure (fig. 10d), 50 m from the Hueco Bolson fissure (fig. 10b) and 50 m from the Ryan Flat fissure (fig. 10g) although chloride concentrations were high in these profiles also (fig. 6c, f, and l, and 7f). High tritium concentrations were found beneath the chloride fronts in the Hueco Bolson and Eagle Flat fissure profiles.

Stable isotopes of oxygen and hydrogen were less enriched in profiles in fissures relative to those adjacent to fissures (fig. 11, table 10). This suggests less evaporation of the water in fissured sediments than in nonfissured sediments. In HBF 50m, EFF92 0m, and EFF96 10m profiles, the surface samples were much more enriched than deeper samples. Statistical tests that omitted the surface samples showed that the differences in $\delta^{18}O$ between fissured and nonfissured sediments were significant at $\alpha = 0.05$.

Electromagnetic Induction

Three different fissures, the Eagle Flat fissure (fig. 12b and c), a section of the Red Light Bolson fissure (fig. 12e), and the Ryan Flat fissure (fig. 12f and g), showed higher apparent electrical conductivities in the vicinity of the fissure than in the area adjacent (table 11). In each case, the apparent electrical conductivity measured with the EM31 instrument increased by a factor of approximately 2 in the vicinity of the fissure in both the vertical and horizontal dipole modes. The EM38 instrument was used only at the Ryan Flat fissure, and apparent electrical conductivity mapped with the EM38 also showed increases in the vicinity of the fissure by a factor of 2 in the

horizontal dipole mode and by a factor of 3 in the vertical dipole mode (fig. 12g). The other fissures, the Hueco Bolson fissure (fig. 12a) and another section of the Red Light Bolson fissure (fig. 12d), showed negligible variation in apparent electrical conductivity in the vicinity of the fissure. This section of the Red Light Bolson fissure differs from the other in that its width/depth ratio is much greater and probably represents a less active section of the fissure. The previously discussed borehole data are from the older section of the fissure. Two transects were conducted on the Eagle Flat fissure, one where there was a gully at the surface to mark the location of the fissure (fig. 12b), and a second parallel to the first but with no gully present (fig. 12c). The apparent electrical conductivity along the second transect was similar to the first and indicates that this technique may be suitable for mapping increased subsurface water flux prior to development of surface collapse features associated with fissures.

Apparent electrical conductivities measured with the EM31 meter in the vertical dipole mode were higher than conductivities measured in the horizontal dipole mode in all transects (fig. 12, table 11). These data indicate that electrical conductivity increased with depth. The two transects (VD and HD) generally parallel each other. The increase in apparent electrical conductivity with depth is also consistent with higher conductivities measured with the EM31 relative to those measured with the EM38 in the Ryan Flat fissure because of the differences in the exploration depths of these instruments (fig. 12g).

The apparent electrical conductivity of the unsaturated zone varies with texture, water content, salinity, mineralogy, and structure of the sediments. Rhoades et al. (1989) developed a model to describe the electrical conductivity of sediment in terms of mobile (parallel pathway) and immobile (series pathway) water. The apparent electrical conductivity of the unsaturated zone is proportional to the conductivity of the pore water when the solution conductivity is high relative to the solid phase conductance, generally at solution conductivities ≥ 400 mS m^{-1}. In this case, the following linear model can be used to describe variations in the apparent electrical conductivity of the sediment:

$$EC_a = EC_w \theta \tau + EC_s \qquad (1)$$

where EC_w is the pore-water conductivity, θ is volumetric water content, τ is the tortuosity, and EC_s is the surface conductivity of the sediment. This model applies when the water content is above a certain threshold value. Below this threshold value, EC_w is 0 and the apparent electrical conductivity is controlled by the surface conductivity of the sediment.

Higher apparent electrical conductivity across some fissures indicates that variations in water content rather than chloride concentrations control differences in apparent electrical conductivity across these fissures. If chloride concentrations were controlling apparent electrical conductivity, conductivity values should be reduced across fissures because chloride is flushed out. Because measured apparent electrical conductivity is controlled mostly by variations in water content, this is not a very useful method for detecting higher water fluxes beneath fissures because water content varies also with texture and increased water content is not highly characteristic of fissured sediments. Low chloride concentrations provide a more distinctive signature of high water flux in fissured sediments. The lack of variation in apparent electrical conductivity in some fissures (Hueco Bolson and a section of Red Light Bolson) is attributed to water content being too low to conduct electricity. This is supported by comparisons of downhole electrical conductivity measurements with an EM39 instrument and measured water content, which shows that the threshold water content is approximately 0.07 g g^{-1} (Paine et al., 1995). The EM induction measurements were done in 1994, when precipitation was much lower than the long-term mean annual precipitation. Differences in EC_a between fissured and nonfissured sediments may be much greater after long wet periods.

DISCUSSION

Unsaturated Flow in Fissured Sediments

The physical and chemical data are consistent and show that subsurface water fluxes are higher in fissured sediments than in nonfissured sediments. Higher water potentials, lower chloride concentrations, high tritium levels, less enriched stable isotopes in profiles in fissured

sediments relative to adjacent profiles in nonfissured sediments indicate increased water flux beneath the fissures. A variety of fissures were examined in this study. Hydraulic and chemical parameters vary within short intervals along the Eagle Flat fissure, indicating that there is almost as much variability along individual fissures as there is between fissures. The different profiles in the Eagle Flat fissure indicate different degrees of flushing of the pore-water chloride, which may be related to small-scale topographic changes along the fissure.

Preferential Flow

Because surface fissures intercept drainage, water ponds on these features and focuses subsurface flow in the shallow zone. Although some researchers refer to *focused flow* as a macroscopic-scale preferential flow (Gee and Hillel, 1988), most workers restrict the term *preferential flow* to flow along macropores and/or unstable flow. Previous tracer experiments conducted on fissures indicate preferential flow in fracture-fill material (Scanlon, 1992b). High tritium concentrations found throughout the sampled fissure profiles may simply reflect enhanced water flux associated with ponding in the fissures. Penetration of ^3H below chloride fronts in the Hueco Bolson and Eagle Flat fissures may reflect preferential flow of water or may reflect the difference between vapor transport of tritiated water relative to liquid transport of chloride. If preferential transport of water containing tritium and chloride (~ 10%) occurs ahead of the main solute front and this water mixes with the stored water ahead of the main solute front, the resultant tritium and chloride concentrations below the solute front can be estimated using mixing calculations according to the following:

$$C_{mix} = V_p C_p + V_m C_m \qquad (2)$$

where C_{mix}, C_p, and C_m are concentrations of tritium or chloride in the mixture, preferentially moving water, and matrix water, respectively, V_p and V_m are the fractional volumes of preferentially moving water and matrix water, respectively, and sum to 1. Mixing 10% water that has bomb pulse tritium (estimated 100 TU) with 90% matrix water stored ahead of the main solute front that has negligible tritium (estimated ~ 0.01 TU) results in 10 TU in the mixture. Mixing 10%

low chloride water (~ 10 g m^{-3}) that is flowing preferentially ahead of the chloride front with 90% of the in situ high chloride (~ 5,500 g m^{-3}) water ahead of the front results in a concentration of 4,951 g m^{-3} in the mixture. The above simple example shows how the tritium levels in water may be greatly affected by preferential flow of bomb pulse water, whereas the chloride concentrations of the pore water should be negligibly affected by preferential flow because the chloride signature of preferentially flowing water is masked by the high chloride concentrations of the pore water ahead of the solute front. Lateral flow as suggested by dilution of chloride in the EFF36 profile 10 m from the fissure may account in part for the tritium levels in the profile 10 m from the fissure.

Vapor transport may also account for deeper penetration of tritium relative to chloride. Previous studies that compared the relative penetration depths of ^{36}Cl and ^{3}H attributed deeper penetration of ^{3}H than ^{36}Cl to vapor transport as a result of thermal vapor diffusion; however, these studies were restricted to the upper meter of the unsaturated zone where temperature gradients are steep (Phillips et al., 1988, Scanlon and Milly, 1994). Tritium is deeper beneath the fissures ($\leq$ 26 m depth), and temperature gradients are negligible at these depths. Analysis of steady state diffusion of tritium with a concentration of 100 TU at the upper boundary decays to a value of 0.37 times the bounding value at a depth of 0.3 m (Appendix 1). This analysis indicates that vapor diffusion alone cannot account for the much deeper penetration of tritium relative to chloride beneath the fissures. Smiles et al. (1995) also showed that diffusion of tritium in the vapor phase is limited by equilibration between the liquid and gas phases because the concentration of tritium is 5 orders of magnitude less in the vapor phase than in the liquid phase, reflecting the different densities of water molecules in the two phases. The liquid phase, therefore, acts as a large sink for tritium. Smiles et al. (1995) suggest that barometric pumping should have a negligible effect on tritium concentrations in the unsaturated zone because of the low concentrations of tritium in the vapor phase and rapid equilibration with the liquid phase. High tritium values (e.g., 1,100 TU at 24 m depth, $\leq$ 162 TU at 109 m depth) have been found adjacent to the Beatty site, Nevada, that cannot readily be explained by liquid or combined liquid and vapor transport (Prudic and Striegl,

1995; Striegl et al., 1996). Until we have a better understanding of vapor transport of tritiated water we cannot assess the significance of the presence of tritium.

Preferential flow is indicated by partial flushing of chloride and moderately high chloride concentrations in some profiles (EFF88 0m and EFF92 0m) beneath the Eagle Flat fissure. In contrast, very low chloride concentrations in EFF35 0m and EFF120 0m indicate that chloride was almost completely flushed out. The water potential and chloride fronts in EFF35 0m in the Eagle Flat fissure are very sharp and suggest that water may be flowing like a piston. Previous studies have used the relative positions of water potential and chloride fronts to evaluate pistonlike flow (Jolly et al., 1989) and have shown that the ratio of the velocities of solute and wetting fronts (R) based on one-dimensional analytical solutions (Warrick et al., 1971) is expressed as

$$R = \frac{\theta_{wet} - \theta_{dry}}{\theta_{wet}} \tag{3}$$

where θ_{wet} is the water content in the wetted portion of the profile and θ_{dry} is the initial water content ahead of the wetting front. The above analysis indicates that under pistonlike flow conditions the solute front should lag behind the wetting front by an amount equal to the amount of initial water in the profile prior to infiltration. If we assume that the water content in the profile 10 m from the Eagle Flat fissure (EFF36 10m) represents the initial water content (θ_{dry}, 0.11 $m^3\ m^{-3}$) in the upper 10 m of the profile beneath the fissure (EFF35 0m), and that θ_{wet} is the mean water content in the upper 10 m of EFF35 0m (0.20 $m^3\ m^{-3}$), then the velocity of the solute front should be about half that of the wetting front. This difference in velocities should result in much greater separation in the water potential and chloride fronts than is found (fig. 6e and f). An alternative explanation of the sharp chloride front beneath the Eagle Flat fissure may be related to the natural capillary barriers created by the distinct layering of sediments in the profile. The depth of the solute front corresponds approximately to an increase in sand content from 13% to 65%. In the presence of natural capillary barriers, water would accumulate on top of the coarse-textured layer until the water potential increased enough to overcome the water entry pressure of the underlying coarse layer. While water was accumulating on the coarse layer, the separation between the wetting and solute fronts would decrease. In addition, the above analysis of the relative

velocities of wetting and solute fronts was based on one-dimensional flow; however, water flow beneath the Eagle Flat fissure may be two-dimensional. Reductions in chloride in EFF36 10m at depth may be related to lateral flow along a capillary barrier. Low chloride concentrations at approximately 5 m depth in EFF88 0m and EFF92 0m may also reflect lateral flow along a capillary barrier, because a sandy layer is found at this depth. Therefore, natural capillary barriers may retard flow and sharpen fronts; however, this does not mean that water movement is pistonlike above the capillary barrier.

Water Flux Estimates

Chloride profiles in fissured sediments cannot be used directly to estimate water fluxes, because the chloride in the profiles may represent residual chloride that reflects incomplete flushing of the chloride and would not, therefore, represent the current flux through the sediments. This is most apparent in profiles EFF88 0m and EFF92 0m. In contrast, the chloride in the profile EFF35 0m and EFF120 0m is much lower and represents more complete flushing.

If the time that fluxes increased in fissured sediments were known, one could estimate the water fluxes from the depth of the solute fronts found in the Eagle Flat and Hueco Bolson fissures. The vegetation lineation associated with the Eagle Flat fissure is clearly visible in aerial photographs taken in 1957 (Jackson et al., 1993); however, the fissure may have been active for a much longer time. Using a minimum age for the fissure results in a maximum water velocity for unsaturated flow in fissured sediments. If we assume that the Eagle Flat fissure has been present for 50 yr and that the chloride front is about 9 m deep, then the resultant water velocity is 180 mm yr^{-1}, with a water flux of 36 mm yr^{-1}, based on an average volumetric water content of 0.2 m^3 m^{-3} (θ_g 0.14 g g^{-1}, bulk density 1,400 kg m^{-3}). If the fissure is much older, the actual water flux may be much less.

A similar analysis was done for the Hueco Bolson fissure on the assumption that this fissure has been present for 50 yr and that the midpoint of the chloride front is 17 m beneath the fissure

and 14 m in the profile 10 m from the fissure. This results in velocities of 340 mm yr^{-1} beneath the fissure and 280 mm yr^{-1} 10 m from the fissure. The average volumetric water content is 0.14 m^3 m^{-3} beneath the fissure and 0.10 m^3 m^{-3} in the profile adjacent to the fissure (assuming a bulk density of 1,400 kg m^{-3}), giving a water flux of 48 mm yr^{-1} beneath the fissure and 28 mm yr^{-1} adjacent to the fissure. A portion of the water is flowing faster than represented by the chloride front, as indicated by the presence of bomb-pulse tritium down to 26 m depth in the profile 10 m distant from the Hueco Bolson fissure. However, the percent of water flowing below the solute front cannot be determined with available data. Water velocities estimated from the tritium data range from 550 mm yr^{-1} directly beneath the fissure (tritium down to 17 m depth) to 840 mm yr^{-1} 10 m distant from the fissure. This assumes that the tritium represents peak fallout in 1963 and uses the period between peak fallout and sampling (1994) to estimate the velocity. Because the percent of water involved in the tritium transport cannot be estimated, water fluxes cannot be calculated from the tritium data.

Comparison of Different Techniques to Evaluate Flow in Fissured Sediments

Several independent lines of evidence were used to evaluate subsurface water fluxes in fissured sediments. The effectiveness of various techniques in delineating unsaturated flow varied. Although water content in sediments is readily measured, only the Eagle Flat area had substantially higher water content beneath the fissure than 10 m away from it. Water content monitoring also showed high water fluxes beneath this fissure after rainfall. In the other fissures, variations in water content with texture masked any small differences in water content that may have occurred between fissure and nonfissure settings. Unsaturated-zone water potential is a much more sensitive indicator of higher water flux beneath fissures than water content. In many profiles the water potentials near the surface in the upper 0.5 to 1 m zone were low and probably reflected drying of these sediments. At greater depths, the water potential profiles in the fissures were up to an order of magnitude greater than water potentials in adjacent profiles.

The significance of these water potential differences depends on the water retention functions of the sediments, which describe the relationship between water potential and water content. Water retention curves were developed for coarse- and fine-textured sediments from the Eagle Flat study area (fig. 13). In coarse-textured sediments like those in the Hueco Bolson, the difference from -0.3 MPa beneath the fissure to ~ -3 MPa in the profile 10 m from the fissure reflects very little change in water content (≤ 0.03 m^3 m^{-3}), because these points are in the steep section of the water retention curve. In contrast, the water potential difference from -0.3 MPa in Eagle Flat fissure to -3 MPa in the profile 10 m from the fissure reflects a large change in water content (~ 0.1 m^3 m^{-3}) for silt loam material and is consistent with the water content differences between fissured and nonfissured sediments found in the Eagle Flat area. Therefore, the significance of the water potential differences with respect to water flux varies with texture. Large water potential differences in coarse-textured sediments may reflect only slight changes in water flux; therefore, water potential differences are much more sensitive indicators of small changes in water flux than water content.

Although fissures examined in this study commonly have dense vegetation along them that can be seen as vegetation lines on aerial photos, variations in predawn plant water potentials were not very good indicators of increased water flux in fissured sediments. Clearly vegetation plays a critical role in removing infiltrated water, as seen in the large temporal variations in water content in the Eagle Flat fissure. Differences in predawn plant water potentials were not as great as those in unsaturated-zone water potentials between fissured and nonfissured sediments. The contrast in mean plant water potentials between the Hueco Bolson fissure (-2.7 MPa) and 50 m from the fissure (-4.8 MPa) was not as great as the contrast in water potential profiles in the unsaturated zone (fig. 6b). Creosote bushes were sampled in the Hueco Bolson because there were no mesquite trees outside the fissure. Although large roots were found in fracture-fill sediments in trenches dug to 6 m depth in this fissure (Scanlon, 1992b), rooting depths for creosote are generally less than 2 m. Therefore, the plants in the Hueco Bolson area may be sampling the shallow subsurface, which is generally drier than deeper sections of the fissure profile. The lack of

information on the sampling depths represented by the plant water potentials makes detailed comparisons of plant- and sediment-water potentials difficult. Root densities are generally greatest near the surface; therefore, high water potentials at greater depths would not be well represented by the plant data. Differences in mean water potentials for unsaturated-zone profiles beneath and adjacent to fissures are not as great as differences in measured water potentials in different depth intervals. Therefore, integrating subsurface water potentials as is done by plants would result in lower differences between fissured and nonfissured sediments.

Chloride concentration in pore water is a reliable indicator of unsaturated flow in fissured sediments. All profiles beneath the fissure, and in some cases those 10 m from the fissure, had low chloride concentrations. Chloride is extremely soluble and is readily flushed out of the sediments; however, chloride in pore water takes a long time (up to thousands of years) to accumulate. Because of the above, the low chloride concentrations in some fissures may be a relict of higher water fluxes in the past and may not represent current conditions. This may be the case in the mature fissures, such as the Red Light Bolson fissure, where low water potentials indicate that the sediments are dry.

Tritium was detected in all samples analyzed for tritium beneath and adjacent to fissures. The maximum vertical or lateral extent of high trituim cannot be determined from these data. As discussed previously, the significance of the high tritium levels cannot readily be determined. Stable isotopes of oxygen and hydrogen suggest less enrichment of the water directly beneath the fissures. Differences in the isotope concentrations were not as marked as the differences in water potential and chloride concentrations.

The ^{36}Cl data indicated little bomb-pulse signature in the profiles through the fissured sediments. This may result from dilution of the bomb-pulse signature with old residual chloride that was incompletely flushed from the system, or it may reflect post-1980 water because ^{36}Cl concentrations returned to prebomb levels in the 1980s. Because zones of high flux are associated with low chloride concentrations, it is difficult to collect enough chloride for analysis of ^{36}Cl;

therefore, ^{36}Cl is generally not considered a suitable tracer for delineating flow in fissured sediments.

Electromagnetic induction is of limited use in defining flow in fissured sediments because the primary control on apparent electrical conductivity variations is water content, and water content variations are not very characteristic of flow in fissured sediments. In natural interfluvial settings in arid regions, water fluxes and resultant water contents are extremely low and the conductivity corresponding to the water is essentially zero. This corresponds to the threshold water contents of 0.05 $m^3\ m^{-3}$ for a sand and 0.12 $m^3\ m^{-3}$ for a clay determined by Rhoades et al. (1976). Slightly higher water contents beneath the Eagle Flat fissure register as higher apparent electrical conductivity.

Water content monitoring in the Eagle Flat fissure indicates that flow in fissured sediments varies with rainfall. The borehole sampling data in this study represent the results of collection at one time and cannot be used to evaluate temporal variations in flow in fissured sediments. In addition, most of the sampling was done in 1994 (table 1), an unusually dry year in which annual precipitation was about 40% of the long-term mean values. This sample bias may account for the small differences in some of the hydraulic parameters such as water content, water potential (particularly plant water potential), and apparent electrical conductivity between fissured and nonfissured sediments, but it should not affect differences in environmental tracer distributions such as chloride and tritium, because these tracers represent long-term net water fluxes. Considering these factors, sampling should be conducted after long wet periods to maximize differences in hydraulic parameters between fissured and nonfissured sediments.

Implications for Waste Disposal in Arid Settings

Results from the Eagle Flat fissure indicate that the vertical and lateral extent of high water fluxes is limited. Distinct wetting and solute fronts beneath the Eagle Flat fissure show that high water fluxes are restricted to the upper 6 to 10 m of the subsurface. Detailed analyses in a trench

showed that the lateral extent of increased water flux is about 2 m. The vertical extent of high water fluxes was restricted to the upper 20 m beneath and 10 m from the Hueco Bolson fissure as evidenced by chloride fronts. This limited vertical extent of high water fluxes has important implications for waste disposal because it suggests that these fissures do not recharge the underlying aquifer.

Although the high water fluxes associated with fissured sediments in this study were of limited vertical extent, this may not be true of fissures in other settings. It is therefore prudent that sites be properly evaluated for the presence or abence of fissures. Scientists with expertise in geomorphology should carefully review aerial photographs to identify linear features, such as alignments of vegetation, that may indicate fissures. Field examination is essential to determine whether surface depressions and soil pipes are present, and excavations and other tests are required to verify that a feature having significant depth is present. In areas of dense vegetation, field studies are especially important because the vegetation may obscure the presence of fissures on aerial photographs. Once the fissure has been identified, hydrologic studies should be conducted to evaluate the effect of the fissure on unsaturated flow. The most sensitive indicators of high water flux in fissures are water potentials and pore-water chloride concentrations in the unsaturated zone. In some cases, higher water contents in fissured sediments result in higher apparent electrical conductivities, which can be detected by electromagnetic induction. Sampling should be conducted after long wet periods to increase differences in hydraulic parameters between fissured and nonfissured sediments. Ideally, monitoring should be conducted for long periods to evaluate the flow dynamics in these systems.

CONCLUSIONS

Higher water potentials and lower chloride concentrations in fissured sediments relative to adjacent nonfissured sediments indicate higher water fluxes beneath fissures. The lateral extent of high water flux ranged from 2 to more than 10 m from fissures but was less than 50 m from the fissures. The vertical extent of high water flux was restricted to 10 to 20 m depth, as indicated by

steep water potential and chloride fronts in two of the four fissures studied. Water flux estimates based on the position of the chloride front and an assumed age of the Hueco Bolson and Eagle Flat fissures of 50 yr ranged from 28 to 48 mm yr^{-1}.

The various techniques used to evaluate flow in fissured sediments differed in their sensitivity to high water fluxes in fissured sediments. Water potential and chloride concentrations were the most sensitive indicators of high water flux. The lower variations in predawn plant water potentials relative to unsaturated zone water potentials between fissured and nonfissured sediments are attributed to plant roots concentrating in near-surface sediments that are generally drier and to the averaging of the unsaturated volume sampled by the roots. Of the isotopes analyzed, tritium indicated high water flux, but ^{36}Cl was generally an unsuitable indicator of high water flux because of the effect of residual chloride in fissured sediments. High tritium levels found throughout the fissured profiles (to a maximum depth of 26 m) and in profiles adjacent to the fissures cannot readily be explained. Deuterium and oxygen-18 were less enriched beneath the fissures than in adjacent profiles; however, differences in the isotope concentrations were not great. Water content was useful in delineating high water flux in only one fissure, and water content monitoring in this fissure showed large temporal variations in water flux. Electromagnetic induction generally maps water content changes and therefore was not a very good indicator of higher water fluxes beneath fissures. Most of the sample collection was conducted in 1994, an unusually dry year. This may have affected the differences in hydraulic parameters between fissured and nonfissured sediments. Multiple independent lines of evidence are required for obtaining a comprehensive understanding of subsurface flow beneath fissures. Multiple profiles drilled in one fissure indicate that substantial variations in hydraulic parameters and tracer distributions along the fissure may be related to amount of ponding at the surface. Although water fluxes in fissured sediments may have important implications for contaminant transport in arid settings, the limited vertical extent (10 to 20 m) of flow shown by some of the fissures in this study relative to the thickness of the unsaturated sections (140 to 220 m) suggests no effect on the aquifer.

ACKNOWLEDGMENTS

This project was funded under the National Low Level Radioactive Waste Disposal Program under Interagency Contract Number DE-AC07-95ID13223. The authors gratefully acknowledge the cooperation of the landowners (Deron Kasparian and El Paso Water Utilities). The assistance of Junnrien Lai in data analysis is gratefully acknowledged. Word processing was by Susan Lloyd. Layout was by Jamie Coggin.

REFERENCES

Allison, G. B., and Hughes, M. W., 1978, The use of environmental chloride and tritium to estimate total recharge to an unconfined aquifer: Australian Journal of Soil Research, v. 16, p. 181–195.

Allison, G. B., Stone, W. J., and Hughes, M. W., 1985, Recharge in karst and dune elements of a semi-arid landscape as indicated by natural isotopes and chloride: Journal of Hydrology, v. 76, p. 1–26.

ASTM D-5298-92, 1992, The filter paper method: American Society for Testing Materials.

Baumgardner, R. W., Jr., and Scanlon, B. R., 1992, Surface fissures in the Hueco Bolson and adjacent basins, West Texas: The University of Texas at Austin, Bureau of Economic Geology Geological Circular 92-2, 40 p.

Bentley, H. W., Phillips, F. M., and Davis, S. N., 1986, ^{36}Cl in the terrestrial environment, *in* Fritz, P., and Fontes, J.-C., eds., Handbook of environmental isotope geochemistry: New York, Elsevier Science, v. 2b, p. 422–475.

Boling, J. K., 1986, Earth-fissure movements in south-central Arizona, U.S.A., in Johnson, A. I., Carbognin, L., and Ubertini, L., eds., Land subsidence: Proceedings of the Third International Symposium on Land Subsidence, Venice, Italy, March 19–25, 1984: International Association of Hydrological Sciences Publication No. 151, p. 757–766.

Campbell, G. S., 1985, Soil physics with BASIC: Transport models for soil-plant systems: New York, Elsevier, 150 p.

Edmunds, W. M., and Walton, N. R. G., 1980, A geochemical and isotopic approach to recharge evaluation in semi-arid zones: past and present, *in* Arid zone hydrology, investigations with isotope techniques: Vienna, IAEA, IAEA-AG-158/4, p. 47–68.

Elmore, D., Conard, N. J., Kubik, P. W., and Fabryka-Martin, J., 1984, Computer controlled isotope ratio measurements and data analysis: Nuclear Instruments and Methods in Physics Research, Section B, v. 5, p. 233–237.

Folk, R. L., 1974, Petrology of sedimentary rocks: Austin, Texas, Hemphill, 182 p.

Gee, G. W., and Bauder, J. W., 1986, Particle-size analysis, *in* Page, A. L., ed. Methods of soil analysis, part 2, chemical and mineralogical methods: Madison, Wisconsin, American Society of Agronomy, p. 383–410.

Gee, G. W., and Hillel, D., 1988, Groundwater recharge in arid regions: review and critique of estimation methods: Hydrological Processes, v. 2, p. 255–266.

Greacen, E. L., Walker, G. R., and Cook, P. G., 1987, Evaluation of the filter paper method for measuring soil water suction, *in* International Conference on Measurement of Soil and Plant Water Status: Logan, Utah, p. 137–143.

Ingraham, N. L., and Shadel, C., 1992, A comparison of toluene distillation and vacuum/heat method for extracting soil water for stable isotopic analysis: Journal of Hydrology, v. 140, p. 371–387.

Jackson, M. L. W., Langford, R. P., and Whitelaw, M. J., 1993, Basin-fill stratigraphy, Quaternary history, and paleomagnetics of the Eagle Flat study area, southern Hudspeth County, Texas: The University of Texas at Austin, Bureau of Economic Geology final contract report prepared for the Texas Low-Level Radioactive Waste Disposal Authority, 137 p.

Jolly, I. D., Cook, P. G., Allison, G. B., and Hughes, M. W., 1989, Simultaneous water and solute movement through an unsaturated soil following an increase in recharge: Journal of Hydrology, v. 111, p. 391–396.

Lang, A. R. G., 1967, Osmotic coefficients and water potentials of sodium chloride solutions from 0 to 40 C: Australian Journal of Chemistry, v. 20, p. 2017–2023.

Larson, M. K., and Pewe, T. L., 1986, Origin of land subsidence and earth fissuring, northeast Phoenix, Arizona: Association of Engineering Geologists Bulletin, v. 23, no. 2, p. 139–165.

McNeill, J. D., 1992, Rapid, accurate mapping of soil salinity by electromagnetic ground conductivity meters, *in* Advances in measurement of soil physical properties: bringing theory into practice: Soil Science Society of America Special Publication no. 30, p. 209–229.

Paine, J. G., Goldsmith, R. S., and Scanlon, B. R., 1995, Electrical conductivity and gamma ray response to clay, water and chloride content in fissured sediments, Trans-Pecos, Texas: The University of Texas at Austin, Bureau of Economic Geology, contract report, variously paginated.

Phillips, F. M., 1994, Environmental tracers for water movement in desert soils of the American Southwest: Soil Science Society of America Journal, v. 58, p. 14–24.

Phillips, F. M., Mattick, J. L., and Duval, T. A., 1988, Chlorine 36 and tritium from nuclear weapons fallout as tracers for long-term liquid movement in desert soils: Water Resources Research, v. 24, p. 1,877–1,891.

Prudic, D. E., and Striegl, R. G., 1995, Tritium and radioactive carbon (^{14}C) analyses of gas collected from unsaturated sediments next to a low-level radioactive-waste burial site south of Beatty, Nevada, April 1994 and July 1995: U.S. Geological Survey Open-File Report 95-741, 7 p.

Rhoades, J. D., Manteghi, N. A., Shouse, P. J., and Alves, W. J., 1989, Soil electrical conductivity and soil salinity: new formulations and calibrations. Soil Science Society of America Journal, v. 53, p. 433–439.

Rhoades, J. D., Raats, P. A. C., and Prather, R. J., 1976, Effects of liquid-phase electrical conductivity, water content, and surface conductivity on bulk soil electrical conductivity: Soil Science Society of America Journal, v. 40, p. 651–655.

Robinson, G. M., and Peterson, D. E., 1962, Notes on earth fissures in southern Arizona: U.S. Geological Survey Circular 466, 7 p.

Scanlon, B. R., 1992a, Evaluation of liquid and vapor water flow in desert soils based on chlorine-36 and tritium tracers in nonisothermal flow simulations: Water Resources Research, v. 28, p. 185–197.

Scanlon, B. R., 1992b, Moisture and solute flux along preferred pathways characterized by fissured sediments in desert soils: Journal of Contaminant Hydrology, v. 10, p. 19–46.

Scanlon, B. R., 1994, Water and heat fluxes in desert soils 1. Field studies: Water Resources Research, v. 30, p. 709–719.

Scanlon, B. R., and Milly, P. C. D., 1994, Water and heat fluxes in desert soils 2. Numerical simulations: Water Resources Research, v. 30, p. 721–733.

Schumann, H. H., Cripe, L. S., and Laney, R. L., 1986, Land subsidence and earth fissures caused by groundwater depletion in southern Arizona, U.S.A., *in* Johnson, A. I., Carbognin, L., and Ubertini, L., eds., Land subsidence: Proceedings of the Third International Symposium on Land Subsidence, Venice, Italy, March 19–25, 1984: International Association of Hydrological Sciences Publication No. 151, p. 841–851.

Slaff, Steven, 1989, Patterns of earth-fissure development: examples from Picacho Basin, Pinal County, Arizona: Arizona Geology, v. 19, no. 3, p. 4–5.

Smiles, D. E., Gardner, W. R., and Shulz, R. K., 1995, Diffusion of tritium in arid disposal sites: Water Resources Research, v. 31, p. 1483–1488.

Striegl, R. G., Prudic, D. E., Duval, J. S., Healy, R. W., Landa, E. R., Pollock, D. W., Thorstenson, D. C., and Weeks, E. P., 1996, Factors affecting tritium and ^{14}Carbon distributions in the unsaturated zone near the low-level radioactive-waste burial site south of Beatty, Nevada: U.S. Geological Survey Open File Report 96-110, 16 p.

U.S. Department of Agriculture, 1975, Soil taxonomy: Washington, D.C., 754 p.

Warrick, A. W., Biggar, J. W., and Nielsen, D. R., 1971, Simultaneous solute and water transfer for an unsaturated soil: Water Resources Research, v. 7, p. 1216–1225.

FIGURES

Figure 1. Location of fissures (modified from Baumgardner and Scanlon, 1992). Inset shows location of boreholes adjacent to Eagle Flat fissure. EFF121 was drilled 0.6 m from and EFF122 was drilled adjacent to EFF55NP and are not shown. NP refers to neutron probe access tube.

Figure 2. Cross section of trench at the (a) Eagle Flat fissure and (b) Hueco Bolson fissure.

Figure 3. View of Eagle Flat fissure on aerial photograph.

Figure 4. Variation in water content with depth and time in neutron probe access tubes in and 10 m distant from Eagle Flat fissure.

Figure 5. Profiles of water content, water potential, chloride, and bromide (EFF121 and EFF122) beneath the pond adjacent to the neutron probe access tube (EFF55NP) in Eagle Flat fissure.

Figure 6. Profiles of water content, water potential, and chloride concentrations in and adjacent to Hueco Bolson and Eagle Flat fissures.

Figure 7. Profiles of water content, water potential, and chloride concentrations in and adjacent to Red Light Bolson and Ryan Flat fissures.

Figure 8. Comparison of predawn plant water potentials measured in and adjacent to fissures.

Figure 9. Spatial variability in chloride concentrations in a trench beneath Eagle Flat fissure.

Figure 10. Variations in ^{3}H and $^{36}Cl/Cl$ in profiles in and adjacent to fissures.

Figure 11. Stable isotopes of oxygen and hydrogen in and adjacent to fissures.

Figure 12. Electromagnetic transects across fissures.

Figure 13. Retention curves for sediment samples from the Eagle Flat study area.

Table 1. Borehole names (0m, 10m, and 50m indicate borehole location in m relative to fissures), date drilled, borehole depths, types of analyses conducted on sediment samples (wc, water content; wp, water potential), monitoring equipment installed, and borehole locations determined by global positioning system (GPS).

Table 2. Chloride water potential, water content, and texture data organized by geomorphic setting.

Table 3. Texture and water content of sediment samples collected beneath and adjacent to fissures.

Table 4. Water content, water potential, chloride, and bromide in samples from boreholes EFF121 0m and EFF122 0m drilled beneath a pond in Eagle Flat fissure.

Table 5. Water content and chloride concentrations of sediment samples in and adjacent to fissures.

Table 6. Gravitational, water, total, and osmotic potentials of sediment samples collected beneath and adjacent to fissures.

Table 7. Water potential measured with the filter paper in samples from the trench beneath Eagle Flat fissure.

Table 8. Predawn plant water potentials measured in and adjacent to fissures.

Table 9. Chloride concentration of sediment samples collected from the trench beneath Eagle Flat fissure.

Table 10. Deuterium and oxygen-18, tritium, and chlorine-^{36}/chlorine ratios in samples collected beneath and adjacent to fissures.

Table 11. Apparent electrical conductivity measured with EM31 and EM38 in vertical and horizontal dipole modes along transects perpendicular to the trends of the fissures.

APPENDIX 1

The governing equation for tritium diffusion in the gas phase is:

$$\frac{\partial C}{\partial t} = \frac{\partial(\theta_g C_g + \theta_l C_l)}{\partial t} = D_0 \theta_g \tau \frac{\partial^2 C_g}{\partial z^2} - \lambda\left(\theta_g C_g + \theta_l C_l\right) \quad (4)$$

where C is the mass of tritiated water per unit volume of soil, θ_g is the volumetric gas content, θ_l is the volumetric liquid content, C_g is the gas concentration (pCi m^{-3} air), C_l is the liquid concentration (pCi m^{-3} water), D_0 is the free air vapor diffusion coefficient, λ is the radioactive decay constant for tritium (0.0559 yr^{-1}). Equation 4 is reduced to one variable (C_g) by relating the gas concentration to the liquid concentration using Henry's Law constant (K_H=17.5 x 10^{-6} at 293 K).

$$C_g = K_H C_l \quad (5)$$

Substituting equation 5 into equation 4 yields:

$$\frac{\partial(\theta_g C_g + \frac{\theta_l}{K_H} C_g)}{\partial t} = D_0 \theta_g \tau \frac{\partial^2 C_g}{\partial z^2} - \lambda\left(\theta_g C_g + \frac{\theta_l}{K_H} C_g\right) \quad (6)$$

$$\frac{\partial C_g}{\partial t} = D^* \frac{\partial^2 C_g}{\partial z^2} - \lambda C_g \quad (7)$$

where $D^* = \frac{D_0 \theta_g \tau}{\theta_g + \theta_l / K_H}$. If we assume that the system is at steady state, i.e. $\frac{\partial C_g}{\partial t} = 0$, equation 7 reduces to:

$$D^* \frac{\partial^2 C_g}{\partial z^2} = \lambda C_g \quad (8)$$

The boundary conditions include a constant concentration at the surface assumed to be 100 TU (3.2 x10^5 pCi m^{-3}) and an infinitely deep unsaturated zone, i.e.

$$C_g(z = 0) = C_0$$

$$\left.\frac{\partial C_g}{\partial z}\right|_{z=\infty} = 0$$

The solution to equation 7 with the above boundary conditions is:

$$\frac{C_g(z)}{C_0} = e^{\left[-\frac{z\sqrt{\lambda}}{\sqrt{D^*}}\right]} \quad (9)$$

Typical values for the parameters for the site are $\theta_g \sim 0.3$, and $\theta_l \sim 0.2$. The tortuosity was estimated from Millington and Quirk (1961) to be ~ 0.25. $D_0 = 810$ m^2 yr^{-1} (Smiles et al., 1995).

$$D^* = \frac{(810\ m^2\ yr^{-1})(0.3)(0.25)}{0.3 + 0.2 / 17.5 \times 10^{-6}} = 0.005\ m^2\ yr^{-1} \qquad (10)$$

The resultant tritium variation with depth is

$$\frac{C_z}{C_0} = e^{\left[-z\sqrt{0.0559/0.005}\right]} = e^{[-z/0.3]}$$

The e folding depth for this exponential function is 0.3 m, which is the depth at which the concentration at the upper surface reduces to e^{-1} (= 0.37) times the value at the surface. Therefore, a value of 100 TU at the surface will reduce to 37 TU at 0.3 m depth and to 0.9 TU at 2 m depth. The results of this exercise show that tritium will not migrate very deeply as a result of vapor diffusion because most of the tritium is in the liquid phase. Vapor diffusion cannot explain the deep penetration of tritium to 26 m depth, which is below the solute front in the fissure (~ 9 m depth) or the migration of tritium to the profile 10 m from the fissure.

Table 1. Borehole locations, date drilled, borehole depths, types of analyses conducted on sediment samples, monitoring equipment installed, and borehole locations determined by global positioning system.

	Borehole name	Date drilled	Total depth (m)	Analyses conducted or monitoring equipment installed	GPS location
Hueco Bolson	HBF 0m	9/7/94	23.9	wc, wp, Cl, ^{36}Cl, ^{3}H, ^{2}H, ^{18}O, texture	31°24'33.094228"N 105°44'8.588454"W
	HBF 10m	9/4/94	27.0	wc, wp, Cl, ^{3}H, texture	31°24'32.810292"N 105°44'8.744034"W
	HBF 50m	9/14/94	10.2	wc, wp, Cl, ^{36}Cl, ^{2}H, ^{18}O, texture	31°24'31.746579"N 105°44'9.387816"W
Eagle Flat	EFF35 0m	10/17/92	21.2	wc, wp, Cl, texture	31°08'25.714526"N 105°17'50.376983"W
	EFF36 10m	10/17/92	30.6	wc, wp, Cl, ^{36}Cl, texture	31°08'25.879344"N 105°17'50.058330"W
	EFF55NP 0m	5/2/93	8.6	neutron probe	31°08'26.065277"N 105°17'50.587232"W
	EFF56NP 10m	5/2/93	8.5	neutron probe	31°08'26.186447"N 105°17'50.266548"W
	EFF59 0m	4/18/93	27.5	wc, wp, Cl, texture	31°08'26.683444"N 105°17'50.484839"W
	EFF88 10m	5/14/93	13.3	wc, wp, Cl, texture	31°08'26.571593"N 105°17'50.921608"W
	EFF92 0m	8/19/94	22.1	wc, wp, Cl, ^{36}Cl, ^{3}H, ^{2}H, ^{18}O, texture	31°08'25.392766"N 105°17'50.174311"W
	EFF96 10m	8/31/94	17.0	wc, wp, Cl, ^{2}H, ^{18}O, texture	31°08'25.563342"N 105°17'49.841705"W
	EFF119 10m	8/3/95	20.3	wc, wp, Cl	31°08'34.791202"N 105°17'58.441426"W
	EFF120 0m	2/17/96	23.5	wc, wp, Cl	31°08'34.612781"N 105°17'58.735824"W
	EFF121 0m	2/27/97	22.9	wc, wp, Cl, Br	31°08'26.065277"N 105°17'50.587232"W
	EFF122 0m	2/25/97	24.5	wc, wp, Cl, Br	31°08'26.065277"N 105°17'50.587232"W
Red Light Bolson	RLBF 0m	8/23/94	20.6	wc, wp, Cl, ^{36}Cl, ^{2}H, ^{18}O, texture	30°59'23.707929"N 105°17'55.307586"W
	RLBF 50m	8/24/94	8.7	wc, wp, Cl, ^{2}H, ^{18}O, texture	30°59'23.361953"N 105°17'53.495987"W
Ryan Flat	RFF 0m	9/3/94	25.3	wc, wp, Cl, ^{36}Cl, ^{3}H, ^{2}H, ^{18}O, texture	30°29'56.255547"N 104°29'15.711996"W
	RFF 10m	9/2/94	16.3	wc, wp, Cl, ^{36}Cl, texture	30°29'55.886799"N 104°29'14.691423"W
	RFF 50m	9/1/94	13.3	wc, wp, Cl, ^{2}H, ^{18}O, texture	30°29'56.888861"N 104°29'13.683509"W

Table 2. Summary of texture, water content, water potential, chloride, chlorine-36, and stable-isotope data of samples from boreholes in and adjacent to fissures.

Fissure	Borehole #	Date drilled	Borehole depth (m)	Gravel %	Sand %	Silt %	Clay %	Water content mean ($g\ g^{-1}$)	Unsaturated zone water potential mean (MPa)	Plant-water potential mean (MPa)	Chloride mean ($g\ m^{-3}$)	$^{36}Cl/Cl$ mean x 10^{15}	^{3}H mean (TU)	δD_{VSMOW} mean (‰)	$\delta^{18}O_{VSMOW}$ mean (‰)
Hueco Bolson	HBF 0m	9/7/94	23.90	6	44	23	27	0.09 (1)	-1.9 (3)	-2.7	22 (1)	448	13.5	-53	-7.1
	HBF10m	9/4/94	27.00	5	55	19	21	0.06 (2)	-4.9 (4)		48 (2)		25.7		
	HBF 50m	9/14/94	10.20	9	48	25	17	0.05	-8.8	-4.8	1623	434	35.5	-42	-1.7
Eagle Flat	EFF35 0m	10/17/92	21.20	2	34	40	24	0.14 (5)	-0.5 (5)	-1.7	N/A				
	EFF36 10m	10/17/92	30.60	0	30	25	45	0.10	-7.7		5628	373			
	EFF59 10m	4/18/93	27.50	2	29	26	42	0.11	-6.4		5911				
	EFF88 0m	5/14/93	13.30	1	36	25	38	0.12 (6)	-1.1 (6)		N/A				
	EFF92 0m	8/19/94	22.10	0	37	24	39	0.09 (7)	-2.4* (7)		1206 (7)	391	18.0	-45	-3.1
	EFF96 10m	8/31/94	17.00	0	41	22	37	0.09	-8.5		4930		17.1	-43	-1.5
	EFF119 10m	8/3/95	23.50					0.09	-6.2		4750				
	EFF120 0m	2/17/96	20.50					0.13 (8)	-0.7 (8)		21 (8)				
	100 m from fissure									-2.0					
Red Light Bolson	RLBF 0m	8/23/94	16.10	9	36	30	25	0.07	-2.7	-2.3	112	713		-55	-7.1
	RLBF 50m	8/24/94	8.70	5	41	29	25	0.05	-5.9	-2.0	2268			-43	-2.0
Ryan Flat	RFF 0m	9/3/94	25.30	3	34	22	41	0.16	-1.4	-1.6	97	575	8.9	-52	-5.4
	RFF 10m	9/2/94	16.30	1	37	25	37	0.12	-3.8		737	544			
	RFF 50m	9/1/94	13.30	0	39	23	38	0.14	-3.2	-3.4	437		20.5	-45	-3.0

BDL, below detection limit of 2 $g\ m^{-3}$ in the supernatant

Calculated mean using samples generally from above the chloride front in the upper (1) 14 m, (2) 12 m, (3) 1 to 12 m, (4)1 to 11 m, (5) 9.1 m, (6) 5.8 m, (7) 5.9 m, and (8) 7.7 m. Mean chloride concentrations were not calculated for EFF35 0m and EFF88 0m because supernatant from many of the samples was below the detection limit. * ≥ 0.6 m depth.

Table 3. Texture and water content of sediment samples collected beneath and adjacent to fissures.

Borehole number	Depth (m)	Gravel %	Sand %	Silt %	Clay %	Soil texture	Water content g g^{-1}
HBF 0m	0.03	1	42	36	21	loam	0.04
	1.30	0	72	14	14	sandy loam	0.05
	2.82	42	33	13	11	muddy sandy gravel	0.03
	4.60	0	83	5	12	loamy sand	0.05
	6.13	10	42	29	18	gravelly mud	0.11
	7.19	58	21	12	9	muddy sandy gravel	0.05
	8.05	0	39	32	29	clay loam	0.15
	9.11	1	65	12	22	sandy clay loam	0.09
	10.07	0	45	32	23	loam	0.10
	11.03	1	54	16	30	sandy clay loam	0.17
	12.16	0	45	25	30	clay loam	0.12
	13.12	0	16	54	29	silty clay loam	0.14
	14.08	0	44	32	24	loam	0.13
	15.21	0	18	35	47	clay	0.17
	16.17	0	25	27	48	clay	0.17
	17.13	0	38	21	41	clay	0.17
	19.05	0	64	14	22	sandy clay loam	0.15
	21.08	1	52	11	37	sandy clay	0.14
	23.23	0	34	25	41	clay	0.17
	mean	6	44	23	27		0.12
	R	**-0.52**	**0.32***	**0.34***	**0.85**		
HBF 10m	0.03	1	52	29	18	sandy loam	0.03
	1.65	72	12	8	7	muddy gravel	0.01
	3.14	6	36	33	25	gravelly mud	0.11
	5.67	71	19	6	3	muddy sandy gravel	0.01
	8.15	0	44	23	33	clay loam	0.13
	10.07	4	62	21	13	sandy loam	0.06
	14.14	0	46	30	24	loam	0.10
	17.13	2	38	17	43	clay	0.17
	23.23	1	50	20	30	sandy clay loam	0.16
	26.14	0	85	5	10	loamy sand	0.04
	0.55	0	38	38	24	loam	0.07
	1.16	0	63	21	16	sandy loam	0.04
	2.62	0	83	11	6	loamy sand	0.01
	3.53	0	65	20	15	sandy loam	0.06
	4.21	0	72	15	13	sandy loam	0.06
	4.72	0	80	11	9	loamy sand	0.01
	5.17	0	74	16	10	sandy loam	0.01
	6.19	0	83	7	10	loamy sand	0.01
	6.45	0	88	5	7	loamy sand	0.02
	7.19	0	60	19	21	sandy clay loam	0.09
	7.59	0	26	46	28	clay loam	0.09
	9.11	0	51	19	30	sandy clay loam	0.08
	11.03	0	60	24	16	sandy loam	0.11
	13.01	0	74	10	16	sandy loam	0.07
	15.15	0	13	45	42	silty clay	0.14
	16.11	0	20	32	48	clay	0.15
	19.05	0	58	19	23	sandy clay loam	0.15
	20.18	0	34	26	40	clay	0.15
	21.08	0	58	10	32	sandy clay loam	0.14
	22.10	0	64	13	23	sandy clay loam	0.16
	24.19	0	78	10	12	sandy loam	0.06
	25.10	0	78	10	12	sandy loam	0.05
	mean	5	55	19	21		0.08
	R	**0.34***	**-0.42**	**0.44**	**0.86**		
HBF 50m	0.03	1	57	28	14	sandy loam	0.04
	3.11	80	14	3	3	gravel	0.01
	7.22	76	16	3	4	muddy sandy gravel	0.01
	8.24	0	39	23	38	clay loam	0.11
	0.49	0	36	39	25	loam	0.06

*correlation not statistically significant at α = 0.05.

Table 3. Texture and water content of sediment samples collected beneath and adjacent to fissures.

Borehole number	Depth (m)	Gravel %	Sand %	Silt %	Clay %	Soil texture	Water content g g^{-1}
HBF 50m	1.13	0	64	20	16	sandy loam	0.03
	1.58	0	62	22	16	sandy loam	0.04
	2.04	0	52	26	22	sandy clay loam	0.02
	2.65	0	65	18	17	sandy loam	0.02
	4.18	0	26	50	24	loam	0.07
	4.63	0	48	32	20	loam	0.07
	5.29	0	50	39	11	loam	0.07
	5.70	0	70	24	6	sandy loam	0.04
	6.16	0	63	22	15	sandy loam	0.05
	6.74	0	76	14	10	sandy loam	0.02
	7.68	0	25	45	30	clay loam	0.11
	9.31	0	58	22	20	sandy clay loam	0.09
	mean	9	48	25	17		0.05
	R	**-0.46***	**-0.16***	**0.64**	**0.74**	**.**	
EFF35 0m	0.29	2	41	30	27	clay loam	0.10
	0.59	0	40	36	24	loam	0.11
	0.90	0	49	30	22	loam	0.11
	1.26	1	55	25	19	sandy loam	0.12
	1.57	1	44	31	24	loam	0.15
	1.87	0	31	46	24	loam	0.19
	2.18	0	22	53	25	silt loam	0.16
	2.58	1	30	45	24	loam	0.17
	2.82	0	36	42	22	loam	0.16
	3.12	1	48	33	18	loam	0.15
	3.43	0	31	47	22	loam	0.20
	3.73	1	37	37	25	loam	0.15
	4.10	2	43	34	21	loam	0.14
	4.37	4	46	29	22	loam	0.13
	4.68	2	50	26	21	sandy clay loam	0.13
	4.95	33	49	11	7	muddy sandy gravel	0.07
	5.41	0	90	6	4	sand	0.04
	5.93	4	51	25	20	sandy clay loam	0.11
	6.23	0	53	18	30	sandy clay loam	0.12
	6.54	0	21	45	34	clay loam	0.19
	7.09	0	28	47	25	loam	0.16
	7.76	0	29	40	30	clay loam	0.15
	8.21	0	14	42	44	silty clay	0.16
	8.73	0	42	36	22	loam	0.13
	9.16	0	42	31	26	loam	0.13
	9.68	0	13	52	34	silty clay loam	0.19
	10.32	0	65	18	17	sandy loam	0.08
	10.71	0	3	66	30	silty clay loam	0.21
	11.32	0	31	49	20	loam	0.15
	11.84	0	24	57	19	silt loam	0.16
	12.88	0	50	32	18	loam	0.08
	13.40	2	26	38	33	clay loam	0.09
	14.31	0	15	58	27	silty clay loam	0.15
	14.95	0	18	60	21	silt loam	0.15
	15.86	1	18	60	22	silt loam	0.17
	16.54	3	19	56	23	silt loam	0.14
	17.42	0	32	48	20	loam	0.13
	18.09	8	16	48	29	gravelly mud	0.13
	18.91	0	15	56	29	silty clay loam	0.17
	19.46	0	13	60	27	silty clay loam	0.17
	20.47	0	19	58	23	silt loam	0.16
	mean	2	34	40	24		0.14
	R	**-0.35**	**-0.75**	**0.77**	**0.53**		
EFF36 10m	0.59	0	36	19	45	clay	0.05
	1.05	0	54	23	23	sandy clay loam	0.06
	1.36	0	32	24	44	clay	0.10

*correlation not statistically significant at α = 0.05.

Table 3. Texture and water content of sediment samples collected beneath and adjacent to fissures.

Borehole number	Depth (m)	Gravel %	Sand %	Silt %	Clay %	Soil texture	Water content g g^{-1}
EFF36 10m	1.97	0	30	21	48	clay	0.12
	2.27	0	26	23	50	clay	0.10
	2.58	0	28	21	50	clay	0.08
	2.91	0	35	24	41	clay	0.09
	3.22	0	50	20	30	sandy clay loam	0.09
	3.52	0	27	20	52	clay	0.11
	3.83	1	39	24	37	clay loam	0.09
	4.13	1	47	20	33	sandy clay loam	0.09
	4.47	2	45	20	32	sandy clay loam	0.09
	4.77	1	66	12	21	sandy clay loam	0.05
	5.07	1	62	20	17	sandy loam	0.05
	5.47	0	72	14	14	sandy loam	0.04
	6.02	0	54	25	22	sandy clay loam	0.07
	6.32	0	63	19	18	sandy loam	0.06
	6.63	0	26	28	45	clay	0.11
	6.93	0	25	23	52	clay	0.12
	7.30	0	23	24	52	clay	0.11
	7.70	0	26	27	47	clay	0.12
	8.21	0	41	23	36	clay loam	0.09
	8.67	0	5	39	57	clay	0.14
	9.25	0	31	44	25	loam	0.06
	9.86	0	16	39	45	clay	0.11
	10.35	0	24	34	43	clay	0.11
	10.81	0	4	27	69	clay	0.17
	11.29	0	34	16	49	clay	0.19
	11.96	0	23	17	60	clay	0.14
	12.36	0	26	19	55	clay	0.14
	12.85	0	45	24	30	clay loam	0.07
	13.27	1	34	27	39	clay loam	0.10
	14.10	0	24	27	48	clay	0.12
	14.52	0	17	29	54	clay	0.13
	15.47	0	19	24	58	clay	0.15
	16.08	0	18	24	58	clay	0.16
	17.02	0	17	24	60	clay	0.16
	17.63	0	27	23	50	clay	0.14
	18.58	1	19	25	55	clay	0.15
	19.19	0	29	25	46	clay	0.12
	19.95	0	20	23	57	clay	0.16
	20.86	0	13	26	60	clay	0.16
	22.17	1	11	20	68	clay	0.18
	23.76	0	13	29	58	clay	0.17
	25.31	0	13	31	55	clay	0.16
	26.87	0	10	32	58	clay	0.15
	28.42	0	10	36	54	clay	0.17
	29.98	0	13	32	55	clay	0.17
	mean	0	30	25	45		0.12
	R	**-0.25***	**-0.84**	**0.26***	**0.88**		
EFF59 10m	0.22	0	32	26	42	clay	0.11
	0.53	0	41	20	39	clay loam	0.09
	0.92	0	45	21	34	clay loam	0.07
	1.29	0	45	22	33	clay loam	0.07
	1.56	10	61	11	18	gravelly muddy sand	0.04
	1.90	0	27	26	46	clay	0.10
	2.20	0	24	26	49	clay	0.09
	2.60	0	27	24	49	clay	0.09
	2.84	1	31	24	44	clay	0.09
	3.15	0	36	25	38	clay loam	0.09
	3.45	1	36	27	36	clay loam	0.09
	3.76	0	29	35	36	clay loam	0.09
	4.06	2	45	22	31	sandy clay loam	0.08

*correlation not statistically significant at α = 0.05.

Table 3. Texture and water content of sediment samples collected beneath and adjacent to fissures.

Borehole number	Depth (m)	Gravel %	Sand %	Silt %	Clay %	Soil texture	Water content g g^{-1}
EFF59 10m	4.58	0	24	33	43	clay	0.08
	4.88	1	53	22	24	sandy clay loam	0.06
	5.19	5	73	9	14	gravelly muddy sand	0.04
	5.95	63	22	6	8	muddy sandy gravel	0.03
	6.26	0	6	38	56	clay	0.14
	6.56	1	28	29	41	clay	0.11
	6.87	0	19	26	55	clay	0.13
	6.96	0	32	23	44	clay	0.10
	7.51	1	20	37	42	clay	0.10
	7.90	0	35	27	38	clay loam	0.09
	8.21	0	49	23	29	sandy clay loam	0.07
	9.76	0	17	32	51	clay	0.12
	11.13	0	7	29	63	clay	0.16
	11.83	0	13	21	66	clay	0.12
	12.69	2	30	24	45	clay	0.12
	14.24	0	17	28	55	clay	0.14
	15.80	0	16	26	58	clay	0.15
	17.35	0	24	42	34	clay loam	0.09
	18.91	0	12	32	56	clay	0.15
	20.46	0	16	26	58	clay	0.17
	22.01	0	12	28	60	clay	0.17
	25.21	0	19	34	47	clay	0.13
	26.68	0	19	37	44	clay	0.13
	mean	2	29	26	42		0.10
	R	**-0.42**	**-0.80**	**0.58**	**0.91**		
EFF88 0m	0.22	0	41	26	32	clay loam	0.09
	0.53	0	31	27	41	clay	0.08
	1.10	1	44	22	33	clay loam	0.09
	1.41	0	27	29	43	clay	0.14
	1.71	0	37	23	40	clay	0.16
	2.02	0	27	23	50	clay	0.15
	2.34	0	26	21	52	clay	0.14
	2.96	1	36	27	37	clay loam	0.18
	3.57	1	28	27	44	clay	0.15
	3.89	2	37	29	32	clay loam	0.12
	4.21	4	55	18	23	sandy clay loam	0.09
	4.52	3	57	18	22	sandy clay loam	0.09
	4.82	0	58	23	18	sandy loam	0.09
	5.13	0	89	4	7	sand	0.04
	5.77	0	63	20	17	sandy loam	0.10
	6.29	0	12	37	51	clay	0.19
	7.06	0	39	21	39	clay loam	0.10
	7.84	0	19	37	43	clay	0.15
	8.59	0	17	33	50	clay	0.14
	9.15	0	10	32	59	clay	0.06
	9.73	0	58	24	18	sandy loam	0.16
	10.95	0	28	24	48	clay	0.13
	11.65	3	20	26	52	clay	0.13
	12.50	0	16	26	58	clay	0.13
	mean	1	36	25	38		0.12
	R	**-0.30***	**-0.50**	**0.55**	**0.43**		
EFF92 0m	0.03	0	30	42	28	clay loam	0.05
	0.46	0	47	26	27	sandy clay loam	0.06
	0.79	0	41	26	33	clay loam	0.06
	1.10	0	49	21	30	sandy clay loam	0.07
	1.40	0	39	26	35	clay loam	0.09
	1.71	0	53	17	30	sandy clay loam	0.09
	2.01	0	28	28	44	clay	0.11
	2.32	0	26	28	46	clay	0.12
	2.62	0	29	21	50	clay	0.13

*correlation not statistically significant at $\alpha = 0.05$.

Table 3. Texture and water content of sediment samples collected beneath and adjacent to fissures.

Borehole number	Depth (m)	Gravel %	Sand %	Silt %	Clay %	Soil texture	Water content g g^{-1}
EFF92 0m	2.93	0	45	20	35	clay loam	0.11
	3.23	0	38	18	44	clay	0.13
	3.54	0	39	22	39	clay loam	0.13
	3.97	0	62	18	20	sandy clay loam	0.09
	4.27	0	58	23	19	sandy loam	0.08
	4.58	0	64	16	20	sandy clay loam	0.09
	4.88	0	50	29	21	loam	0.07
	5.36	0	78	9	13	sandy loam	0.06
	5.49	0	76	11	13	sandy loam	0.07
	5.67	0	83	8	9	loamy sand	0.06
	5.80	0	35	38	27	clay loam	0.12
	6.10	0	20	34	46	clay	0.17
	6.41	0	38	23	39	clay loam	0.14
	6.71	0	30	25	45	clay	0.14
	7.44	0	34	34	32	clay loam	0.11
	7.87	0	52	21	27	sandy clay loam	0.17
	8.35	0	70	14	16	sandy loam	0.06
	8.35	0	15	36	49	clay	0.06
	9.57	0	29	46	25	loam	0.18
	10.18	0	10	35	55	clay	0.08
	10.61	0	42	36	22	loam	0.15
	11.09	0	26	27	47	clay	0.14
	11.53	0	32	21	47	clay	0.15
	12.01	0	28	21	51	clay	0.14
	12.44	0	36	24	40	clay loam	0.09
	12.44	0	25	25	50	clay	0.09
	13.78	0	24	40	36	clay loam	0.14
	15.42	0	20	21	59	clay	0.17
	17.40	0	38	22	40	clay loam	0.10
	20.44	0	16	13	71	clay	0.23
	mean	0	37	24	39		0.12
	R		**-0.54**	**0.03**	**0.62**		
EFF96 0m	0.26	0	49	24	27	sandy clay loam	0.06
	0.64	0	60	17	23	sandy clay loam	0.04
	1.11	0	66	17	17	sandy loam	0.04
	1.72	0	35	25	40	clay	0.11
	2.33	0	17	26	57	clay	0.07
	2.64	0	34	21	45	clay	0.10
	3.25	0	45	21	34	clay loam	0.09
	3.63	0	44	18	38	clay loam	0.09
	4.18	0	54	18	28	sandy clay loam	0.07
	4.79	0	71	13	16	sandy loam	0.05
	5.23	0	56	27	17	sandy loam	0.05
	5.64	0	80	6	14	sandy loam	0.04
	6.54	0	40	17	43	clay	0.12
	7.21	0	23	30	47	clay	0.12
	7.79	0	41	29	30	clay loam	0.08
	8.34	0	26	34	40	clay	0.11
	8.75	0	72	13	15	sandy loam	0.04
	9.19	0	41	27	32	clay loam	0.10
	10.21	0	33	25	42	clay	0.10
	10.84	0	37	20	43	clay	0.11
	11.22	0	31	19	50	clay	0.13
	12.41	0	53	21	26	sandy clay loam	0.07
	13.32	0	26	36	38	clay loam	0.10
	14.11	0	17	23	60	clay	0.15
	15.45	0	17	22	61	clay	0.16
	16.25	0	19	21	60	clay	0.16
	16.67	0	20	22	58	clay	0.15
	mean	0	41	22	37		

*correlation not statistically significant at $\alpha = 0.05$.

Table 3. Texture and water content of sediment samples collected beneath and adjacent to fissures.

Borehole number	Depth (m)	Gravel %	Sand %	Silt %	Clay %	Soil texture	Water content g g^{-1}
	R		**-0.86**	**0.36***	**0.90**		
RLBF 0m	0.03	32	44	15	9	muddy sandy gravel	0.07
	0.47	0	43	28	29	clay loam	0.04
	1.02	0	51	26	23	sandy clay loam	0.03
	1.46	52	27	12	9	muddy sandy gravel	0.02
	2.58	0	57	22	21	sandy clay loam	0.04
	3.19	0	42	27	31	clay loam	0.03
	4.13	0	33	31	36	clay loam	0.07
	4.51	0	49	27	24	sandy clay loam	0.06
	4.95	0	35	36	29	clay loam	0.05
	5.43	0	43	29	28	clay loam	0.05
	6.04	62	28	5	6	muddy sandy gravel	0.01
	7.07	0	21	31	48	clay	0.12
	7.51	0	35	39	26	loam	0.08
	8.15	0	31	46	23	loam	0.09
	9.08	0	64	22	14	sandy loam	0.02
	10.23	65	18	9	8	muddy sandy gravel	0.02
	10.94	0	35	43	22	loam	0.08
	12.10	0	38	48	14	loam	0.06
	13.01	0	29	29	42	clay	0.11
	14.01	0	25	42	33	clay loam	0.11
	16.03	0	32	44	24	loam	0.10
	18.20	0	27	44	29	clay loam	0.11
	20.10	0	24	33	43	clay	0.15
	mean	9	36	30	25		0.07
	R	**-0.49**	**-0.45**	**0.63**	**0.72**		
RLBF 50m	0.03	0	25	49	26	loam	0.01
	0.32	0	35	39	26	loam	0.01
	0.59	0	53	29	18	sandy loam	0.05
	0.76	9	24	38	29	gravelly mud	0.06
	1.23	0	55	27	18	sandy loam	0.02
	1.60	0	68	18	14	sandy loam	0.01
	2.48	61	25	7	7	muddy sandy gravel	0.02
	3.22	4	41	25	31	clay loam	0.08
	4.13	0	37	30	33	clay loam	0.08
	4.57	0	20	40	40	clay	0.10
	5.14	0	56	22	22	sandy clay loam	0.03
	6.17	0	15	32	53	clay	0.13
	7.07	0	48	25	27	sandy clay loam	0.04
	8.18	0	72	19	9	sandy loam	0.03
	mean	5	41	29	25		0.05
	R	**-0.19***	**-0.52***	**0.21***	**0.83**		
RFF 0m	0.03	0	35	23	42	clay	0.21
	0.43	0	47	18	35	sandy clay	0.10
	0.98	0	45	31	24	loam	0.07
	1.37	0	27	30	43	clay	0.13
	1.77	0	26	20	54	clay	0.17
	2.16	0	22	10	68	clay	0.19
	2.50	0	14	10	76	clay	0.21
	2.90	1	38	28	33	clay loam	0.12
	3.29	0	34	25	41	clay	0.14
	4.08	0	23	21	56	clay	0.18
	5.04	0	34	21	45	clay	0.18
	6.05	0	22	15	63	clay	0.16
	7.06	0	24	23	53	clay	0.18
	8.20	0	32	24	44	clay	0.20
	9.10	0	18	39	43	clay	0.17
	10.10	0	56	9	35	sandy clay	0.17
	11.02	0	21	40	38	clay loam	0.20
	12.15	0	55	21	24	sandy clay loam	0.13

*correlation not statistically significant at $\alpha = 0.05$.

Table 3. Texture and water content of sediment samples collected beneath and adjacent to fissures.

Borehole number	Depth (m)	Gravel %	Sand %	Silt %	Clay %	Soil texture	Water content g g^{-1}
RFF 0m	13.17	0	55	23	22	sandy clay loam	0.13
	14.16	41	39	12	8	muddy sandy gravel	0.10
	16.05	0	55	19	26	sandy clay loam	0.14
	17.01	0	12	19	69	clay	0.24
	18.14	0	28	29	43	clay	0.21
	19.10	0	29	28	43	clay	0.20
	20.06	0	24	31	45	clay	0.20
	20.85	15	68	4	13	gravelly muddy sand	0.06
	21.67	0	27	43	30	clay loam	0.16
	23.10	37	53	5	6	muddy sandy gravel	0.04
	24.63	0	23	20	57	clay	0.20
	mean	3	34	22	41		0.16
	R	**-0.58**	**-0.74**	**0.29***	**0.79**		
RFF 10m	0.03	3	33	21	43	clay	0.22
	0.43	0	36	37	27	clay loam	0.08
	0.82	1	29	43	28	clay loam	0.07
	1.28	0	24	33	43	clay	0.12
	1.68	0	21	24	55	clay	0.15
	2.07	0	22	22	56	clay	0.16
	2.47	0	18	21	61	clay	0.18
	3.02	0	36	34	30	clay loam	0.11
	3.41	0	48	25	27	sandy clay loam	0.09
	3.98	0	52	23	25	sandy clay loam	0.10
	5.17	0	36	23	41	clay	0.13
	6.13	0	27	19	54	clay	0.16
	7.10	0	62	14	24	sandy clay loam	0.06
	8.09	4	65	11	20	sandy clay loam	0.07
	9.07	0	24	28	48	clay	0.17
	10.09	0	29	18	53	clay	0.16
	11.02	0	22	45	33	clay loam	0.13
	12.15	0	70	10	20	sandy clay loam	0.08
	14.07	7	61	18	14	gravelly muddy sand	0.06
	16.00	0	28	32	40	clay	0.17
	mean	1	37	25	37		0.12
	R	**-0.23***	**-0.73**	**0.05***	**0.84**		
RFF 50m	0.03	8	70	10	11	gravelly muddy sand	0.12
	0.47	0	30	45	25	loam	0.08
	0.87	0	57	23	20	sandy clay loam	0.05
	1.33	0	17	34	49	clay	0.16
	1.71	0	26	23	51	clay	0.17
	2.15	0	23	22	54	clay	0.17
	2.56	0	23	21	56	clay	0.17
	3.00	0	63	16	21	sandy clay loam	0.08
	3.58	0	69	14	17	sandy loam	0.08
	4.16	0	27	25	48	clay	0.16
	4.53	0	24	24	52	clay	0.18
	5.11	0	27	22	51	clay	0.17
	6.05	0	32	21	47	clay	0.16
	6.96	0	33	24	43	clay	0.15
	7.94	0	53	24	23	sandy clay loam	0.10
	8.92	0	10	26	64	clay	0.22
	10.01	0	37	25	38	clay loam	0.15
	10.99	0	19	25	56	clay	0.21
	11.96	0	48	31	21	loam	0.10
	13.06	0	83	8	9	loamy sand	0.06
	mean	0	39	23	38		0.14
	R	**-0.08***	**-0.84**	**0.17***	**0.92**		

*correlation not statistically significant at α = 0.05.

Table 4. Water content, water potential, chloride, and bromide in samples from boreholes EFF121 (0.6 m from EFF55NP) and EFF122 (adjacent to EFF55NP) drilled beneath pond in Eagle Flat fissure.

Borehole number	Depth (m)	Water potential (MPa)	Depth (m)	Gravimetric water content (g g^{-1})	Chloride (mg Cl kg^{-1} soil)	Chloride (g Cl m^{-3} water)	Bromide (mg Br kg^{-1} soil)	Bromide (g Br m^{-3} water)
EFF121	0.06	-0.69	0.15	0.18	25	144	902	5122
	0.37	-0.69	0.46	0.23	30	129	1205	5235
	0.67	-0.71	0.76	0.29	25	85	1085	3677
	0.98	-0.59	1.07	0.19	12	61	294	1521
	1.58	-0.68	1.68	0.20	418	2085	12	62
	2.19	-1.01	2.29	0.13	460	3625	7	57
	2.50	-1.08	2.59	0.13	377	2840	3	22
	3.11	-0.97	3.20	0.15	301	2020	3	17
	3.72	-0.88	3.81	0.13	246	1823	2	14
	4.02	-0.89	4.11	0.12	200	1662	2	13
	4.63	-0.84	4.72	0.07	107	1597	1	13
	5.24	-0.86	5.33	0.04	76	1731	1	15
	5.55	-0.82	5.64	0.05	55	1123	0	10
	6.16	-0.91	6.25	0.10	180	1864	1	13
	6.77	-0.97	6.86	0.16	360	2224	3	16
	7.07	-1.01	7.16	0.17	487	2913	3	19
	7.68	-1.26	7.77	0.14	513	3543	4	24
	8.29	-1.46	8.38	0.09	423	4816	3	29
	8.60	-1.71	8.69	0.07	294	3950	2	28
	9.51	-1.63	9.60	0.18	635	3587	4	23
	10.73	-1.82	10.82	0.15	677	4638	4	28
	12.25	-2.46	12.34	0.15	708	4596	5	30
	13.78	-2.86	13.87	0.16	757	4865	5	30
	15.30	-3.00	15.39	0.16	793	4860	5	29
	16.82	-3.20	16.92	0.12	569	4584	4	30
	18.35	-3.40	18.44	0.14	723	5048	5	32
	19.87	-3.69	19.96	0.18	971	5421	6	34
	21.40	-3.78	21.49	0.17	941	5470	5	32
	22.92	-3.74	23.01	0.18	964	5417	6	33
EFF122	0.06	-0.79	0.15	0.19	27	139	917	4778
	0.37	-0.78	0.46	0.24	35	145	1448	5967
	0.67	-0.83	0.76	0.22	16	70	603	2727
	1.04	-0.93	1.13	0.16	42	259	46	280
	1.65	-1.30	1.43	0.14	656	4762	5	34
	2.26	-1.30	2.35	0.13	571	4561	4	34
	2.56	-1.11	2.65	0.14	642	4740	4	32
	3.17	-1.26	3.26	0.16	622	3846	5	28
	3.78	-1.26	3.87	0.16	419	2604	3	18
	4.08	-1.53	4.18	0.17	508	3032	3	20
	4.69	-1.15	4.79	0.15	354	2434	2	16
	5.30	-1.20	5.39	0.16	382	2461	3	17
	5.61	-1.24	5.70	0.13	275	2056	2	16
	6.22	-1.28	6.31	0.17	298	1711	2	13
	6.83	-1.40	6.92	0.16	336	2058	2	15
	7.13	-1.49	7.22	0.15	356	2444	2	17
	7.74	-1.50	7.83	0.14	495	3422	3	22
	8.35	-1.64	8.44	0.15	546	3736	3	23
	8.66	-1.52	8.75	0.10	384	3847	3	27
	9.57	-1.99	9.72	0.17	628	3786	4	24
	10.79	-2.63	10.88	0.14	586	4329	4	27
	12.31	-3.08	12.41	0.15	668	4438	4	28
	13.84	-3.16	13.93	0.15	673	4618	4	29
	15.36	-3.26	15.45	0.22	773	3479	5	22
	16.89	-3.23	16.98	0.11	492	4395	3	28
	18.41	-3.26	18.50	0.13	628	4754	4	30
	19.93	-2.89	20.03	0.17	900	5148	6	32
	21.46	-3.27	21.55	0.19	959	5110	6	32
	22.98	-3.17	23.07	0.12	612	5047	4	30
	24.51	-2.82	24.60	0.14	683	5042	4	31

Table 5. Water content and chloride concentrations of sediment samples in and adjacent to fissures.

Borehole number	Depth (m)	Gravimetric water content (g g^{-1})	Chloride (mg Cl kg^{-1} soil)	Chloride (g Cl m^{-3} water)
HBF 0m	0.03	0.035	3.3	94.0
	1.30	0.046	1.6	34.6
	2.82	0.032	1.8	55.3
	3.28	0.031	0.8	24.4
	4.60	0.045	0.6	12.6
	6.13	0.106	1.9	17.5
	7.19	0.049	0.9	17.5
	8.05	0.145	1.1	7.9
	9.11	0.089	0.3	3.7
	10.07	0.101	0.5	4.5
	11.03	0.166	0.4	2.6
	12.16	0.125	0.5	3.9
	13.12	0.140	0.4	3.1
	14.08	0.132	0.3	2.5
	15.21	0.172	24.1	140.3
	16.17	0.166	53.0	320.0
	17.13	0.172	90.0	522.8
	19.05	0.153	147.2	959.2
	21.08	0.142	184.9	1300.0
	23.23	0.168	145.9	866.8
HBF 10m	0.03	0.033	5.4	167.0
	0.55	0.065	2.6	39.4
	1.16	0.044	2.2	48.7
	1.65	0.015	0.7	46.0
	2.62	0.010	0.8	80.8
	3.14	0.114	1.1	9.7
	3.53	0.057	1.4	24.8
	4.21	0.061	1.0	16.6
	4.72	0.013	0.8	62.4
	5.17	0.011	2.4	221.5
	5.67	0.014	0.6	46.9
	6.19	0.014	0.9	64.2
	6.45	0.017	1.3	74.4
	7.19	0.092	0.5	5.4
	7.59	0.093	0.4	4.5
	8.15	0.129	0.5	4.3
	9.11	0.078	0.5	6.5
	10.07	0.062	0.5	7.8
	11.03	0.105	0.3	2.9
	11.99	0.081	2.8	34.1
	13.01	0.070	18.2	259.7
	14.14	0.101	109.5	1084.9
	15.15	0.143	255.8	1791.9
	16.11	0.155	269.3	1738.5
	17.13	0.171	219.4	1281.1
	18.03	0.121	148.4	1229.8
	18.82	0.155	166.8	1077.5
	19.05	0.153	154.5	1009.7
	20.18	0.145	148.6	1023.1
	21.08	0.137	167.7	1225.8
	22.10	0.160	219.7	1370.0
	23.23	0.161	128.6	800.8
	24.19	0.065	62.1	955.6
	25.10	0.053	12.5	236.9
	26.14	0.037	5.7	152.3
HBF 50m	0.03	0.035	2.0	58.0
	0.49	0.057	0.7	12.0
	1.13	0.030	4.5	149.4
	1.58	0.036	23.5	647.6
	2.04	0.016	28.1	1775.3
	2.65	0.016	87.5	5359.9
	3.11	0.010	51.8	5436.9
	4.18	0.069	162.4	2363.8
	4.63	0.075	184.3	2473.3
	5.29	0.070	112.2	1609.7
HBF 50m	5.70	0.043	66.6	1564.9
	6.16	0.049	57.3	1162.7
	6.74	0.021	24.1	1127.6
	7.22	0.015	14.1	969.2
	7.68	0.109	110.4	1010.9
	8.24	0.107	102.5	954.5
	9.31	0.092	84.3	917.5
EFF35 0m	0.29	0.096	BD2	BD2
	0.59	0.106	BD2	BD2
	0.90	0.107	BD2	BD2
	1.26	0.120	BD2	BD2
	1.57	0.149	BD2	BD2
	1.87	0.188	BD2	BD2
	2.18	0.158	BD2	BD2
	2.58	0.171	BD2	BD2
	2.82	0.162	BD2	BD2
	3.12	0.148	BD2	BD2
	3.43	0.197	BD2	BD2
	3.73	0.155	BD2	BD2
	4.10	0.144	BD2	BD2
	4.37	0.135	BD2	BD2
	4.68	0.133	BD2	BD2
	4.95	0.072	BD2	BD2
	5.41	0.042	BD2	BD2
	5.93	0.110	21.6	196.4
	6.23	0.120	BD2	BD2
	6.54	0.193	BD2	BD2
	7.03	0.162	3.0	18.6
	7.09	0.155	BD2	BD2
	7.70	0.130	9.9	75.7
	7.76	0.153	BD2	BD2
	8.15	0.132	3.0	22.7
	8.21	0.157	18.0	114.7
	8.67	0.122	19.4	158.4
	8.73	0.127		
	9.10	0.132	118.1	892.9
	9.16	0.131		
	9.68	0.187	BD2	BD2
	9.71	0.197	568.8	2882.3
	10.32	0.084		
	10.71	0.212		
	11.32	0.152	790.1	5205.3
	11.84	0.158		
	12.27	0.122		
	12.88	0.084		
	13.40	0.094		
	14.31	0.155	784.6	5076.4
	14.95	0.150		
	15.86	0.171		
	16.54	0.141		
	17.42	0.132	651.8	4945.4
	18.09	0.129		
	18.91	0.169		
	19.46	0.166		
	20.47	0.157	823.9	5255.0
EFF36 10m	0.59	0.045	358.9	7915.6
	1.05	0.056	428.3	7582.7
	1.36	0.099	657.7	6670.1
	1.66	0.125	780.4	6243.8
	1.97	0.124	859.6	6954.6
	2.27	0.104	704.6	6748.7
	2.58	0.082	554.0	6733.1
	2.91	0.093	604.6	6473.7
	3.22	0.086	532.5	6197.5
	3.52	0.113	663.4	5875.9

BD2 denotes measurements below the detection limit of 2 g m-3 in the supernatant measured by potentiometric titration

Table 5. Water content and chloride concentrations of sediment samples in and adjacent to fissures.

Borehole number	Depth (m)	Gravimetric water content ($g\ g^{-1}$)	Chloride ($mg\ Cl\ kg^{-1}$ soil)	Chloride ($g\ Cl\ m^{-3}$ water)
EFF36 10m	3.83	0.090	437.0	4860.9
	4.13	0.086	509.9	5905.9
	4.47	0.085	283.9	3330.9
	4.77	0.052	303.3	5782.8
	5.07	0.047	237.5	5046.8
	5.47	0.039	212.0	5383.9
	6.02	0.072	360.2	5012.0
	6.32	0.056	287.2	5119.7
	6.63	0.110	560.7	5083.4
	8.21	0.090	435.4	4840.2
	9.86	0.109	518.9	4745.8
	11.29	0.193	655.6	3405.4
	12.85	0.074	370.5	4996.1
	14.52	0.131	744.2	5663.2
	16.08	0.158	784.0	4967.3
	17.63	0.137	730.6	5314.0
	20.86	0.165	879.5	5335.4
	23.76	0.171	932.1	5448.3
	26.87	0.152	799.5	5263.9
	29.98	0.168	998.7	5946.3
EFF59 10m	0.22	0.107	278.6	2593.2
	0.53	0.088	623.5	7062.3
	0.92	0.073	610.6	8396.2
	1.29	0.073	590.2	8054.2
	1.56	0.042	309.7	7365.5
	1.90	0.105	779.9	7432.8
	2.20	0.094	688.8	7342.0
	2.60	0.086	643.9	7506.6
	2.84	0.093	633.0	6814.5
	3.15	0.093	601.7	6489.4
	3.45	0.088	562.1	6371.1
	3.76	0.088	579.7	6570.7
	4.06	0.076	485.3	6417.8
	4.58	0.085	374.6	4429.5
	4.88	0.063	369.7	5848.3
	5.19	0.041	235.6	5748.2
	5.95	0.034	173.7	5138.1
	6.26	0.137	703.5	5125.4
	6.56	0.109	544.0	5013.8
	6.87	0.131	657.8	5037.7
	6.96	0.103	534.7	5215.1
	7.51	0.104	509.6	4905.6
	7.90	0.093	479.2	5169.3
	8.21	0.071	375.4	5265.9
	9.76	0.124	644.7	5181.6
	11.13	0.159	851.1	5368.2
	11.83	0.124	727.4	5873.7
	12.69	0.121	674.0	5567.8
	14.24	0.139	765.9	5509.6
	15.80	0.153	501.2	3285.7
	17.35	0.093	817.3	8803.9
	18.91	0.145	799.7	5511.8
	20.46	0.168	985.7	5860.7
	22.01	0.174	952.4	5475.3
	23.57	0.150	863.6	5752.8
	25.21	0.131	739.7	5641.7
	26.68	0.134	741.6	5549.6
EFF88 0m	0.22	0.093	15.1	162.1
	0.53	0.080	BD2	BD2
	1.10	0.090	BD2	BD2
	1.41	0.138	BD2	BD2
	1.71	0.160	BD2	BD2
	2.02	0.148	BD2	BD2
	2.34	0.139	37.0	266.7
	2.66	0.160	104.8	653.6

Borehole number	Depth (m)	Gravimetric water content ($g\ g^{-1}$)	Chloride ($mg\ Cl\ kg^{-1}$ soil)	Chloride ($g\ Cl\ m^{-3}$ water)
EFF88 0m	2.96	0.181	79.6	438.9
	3.57	0.145	112.3	774.0
	3.89	0.116	80.7	694.6
	4.21	0.089	65.0	733.0
	4.52	0.090	47.9	532.2
	4.82	0.091	19.4	214.3
	5.13	0.044	BD2	BD2
	5.77	0.096	55.1	572.1
	6.29	0.186	401.3	2160.5
	7.06	0.105	256.5	2453.4
	7.84	0.153	636.5	4157.2
	8.59	0.143	612.6	4272.2
	9.15	0.060	231.0	3870.4
	9.73	0.159	616.5	3867.4
	10.95	0.130	544.4	4195.0
	11.65	0.129	614.9	4753.3
	12.50	0.130	552.2	4244.2
EFF92 0m	0.03	0.050	46.9	933.2
	0.46	0.061	1.5	24.1
	0.79	0.058	4.7	80.2
	1.10	0.069	44.5	643.4
	1.40	0.094	136.2	1452.4
	1.71	0.092	141.3	1535.1
	2.01	0.113	199.6	1759.2
	2.32	0.120	224.5	1872.8
	2.62	0.127	279.7	2202.5
	2.93	0.114	227.3	2002.4
	3.23	0.128	260.8	2036.1
	3.54	0.132	225.7	1710.8
	3.97	0.089	86.1	971.7
	4.27	0.078	74.2	949.0
	4.58	0.086	30.2	350.3
	4.88	0.068	46.8	687.3
	5.36	0.062	67.6	1097.3
	5.49	0.069	74.7	1085.1
	5.67	0.062	80.1	1282.4
	5.80	0.116	168.3	1453.4
	6.10	0.173	289.0	1670.3
	6.41	0.139	266.7	1917.5
	6.71	0.143	345.7	2413.6
	7.44	0.108	346.1	3192.2
	7.87	0.166	588.1	3539.2
	8.35	0.061	238.1	3934.8
	8.96	0.112	458.3	4092.1
	9.57	0.180	690.0	3824.3
	10.18	0.078	295.6	3776.4
	10.61	0.149	614.4	4112.9
	11.09	0.136	539.7	3954.4
	11.53	0.148	629.2	4261.1
	12.01	0.137	596.9	4346.4
	12.44	0.093	398.9	4284.5
	12.92	0.100	456.4	4568.5
	13.78	0.140	614.7	4400.2
	14.21	0.154	697.5	4519.9
	14.51	0.154	700.9	4538.1
	15.00	0.153	674.5	4411.1
	15.42	0.169	738.0	4366.9
	16.48	0.153	659.1	4300.8
	17.40	0.101	439.4	4366.4
	18.46	0.164	759.8	4643.3
	19.38	0.161	743.6	4624.2
	20.44	0.226	1124.8	4969.3
	21.36	0.169	829.8	4917.4
EFF96 10m	0.26	0.063	3.7	58.9
	0.64	0.043	187.3	4327.7

BD2 denotes measurements below the detection limit of 2 g m-3 in the supernatant measured by potentiometric titration

Table 5. Water content and chloride concentrations of sediment samples in and adjacent to fissures.

Borehole number	Depth (m)	Gravimetric water content ($g\ g^{-1}$)	Chloride ($mg\ Cl\ kg^{-1}$ soil)	Chloride ($g\ Cl\ m^{-3}$ water)
EFF96 10m	1.11	0.041	260.7	6357.8
	1.72	0.112	769.9	6875.2
	2.33	0.068	418.2	6176.4
	2.64	0.096	598.7	6249.7
	3.25	0.088	505.5	5760.6
	3.63	0.091	523.4	5723.6
	4.18	0.070	383.3	5508.3
	4.79	0.046	233.1	5106.7
	5.23	0.053	261.5	4891.2
	5.64	0.040	196.2	4910.7
	6.54	0.116	538.0	4654.0
	7.21	0.117	549.9	4713.9
	7.79	0.083	373.5	4475.4
	8.34	0.107	489.4	4577.8
	8.75	0.041	180.1	4398.1
	9.19	0.095	456.4	4783.1
	10.21	0.098	469.5	4784.0
	10.84	0.114	506.1	4441.0
	11.22	0.127	615.1	4825.8
	12.41	0.072	344.5	4782.8
	13.32	0.103	502.2	4887.0
	14.11	0.145	722.4	4973.3
	15.45	0.161	804.0	5001.7
	16.25	0.158	777.6	4912.7
	16.67	0.154	764.4	4960.3
EFF119 10m	0.03	0.053	1.7	32.8
	0.21	0.059	3.6	62.0
	0.40	0.067	71.5	1062.5
	0.58	0.066	240.3	3666.4
	0.76	0.061	326.3	5349.4
	0.94	0.063	314.4	5009.9
	1.28	0.079	421.7	5345.1
	1.65	0.093	494.2	5300.9
	2.01	0.092	520.2	5683.8
	2.38	0.092	549.6	5979.6
	2.62	0.097	565.5	5848.2
	2.99	0.093	546.2	5855.3
	3.35	0.094	550.0	5881.5
	3.72	0.091	516.9	5658.5
	4.08	0.125	690.3	5508.9
	4.33	0.120	615.6	5139.8
	4.69	0.096	519.5	5406.7
	5.61	0.061	303.9	4975.5
	6.40	0.031	139.9	4561.3
	8.29	0.098	430.6	4384.3
	10.00	0.052	220.1	4233.4
	10.97	0.046	210.5	4542.5
	12.37	0.145	686.9	4734.1
	13.29	0.127	649.9	5112.6
	15.12	0.143	680.9	4775.9
	16.95	0.165	821.4	4981.7
	18.78	0.176	881.3	5006.4
	19.99	0.092	479.6	5218.9
EFF120 0m	0.02	0.146	22.5	154.9
	0.17	0.103	3.2	31.0
	0.32	0.113	3.2	28.6
	0.47	0.126	1.7	13.8
	0.62	0.121	1.8	15.2
	0.69	0.124	2.1	17.0
	0.99	0.128	2.0	15.5
	1.30	0.098	1.0	9.8
	1.60	0.122	0.6	4.9
	1.91	0.126	1.2	9.4
	2.21	0.137	1.5	11.0
	2.97	0.189	2.0	10.6

Borehole number	Depth (m)	Gravimetric water content ($g\ g^{-1}$)	Chloride ($mg\ Cl\ kg^{-1}$ soil)	Chloride ($g\ Cl\ m^{-3}$ water)
EFF120 0m	3.73	0.123	1.7	14.0
	4.50	0.151	0.5	3.4
	5.26	0.154	1.2	8.0
	6.02	0.160	1.2	7.8
	6.78	0.135	1.5	11.4
	7.54	0.155	2.0	12.6
	8.31	0.161	25.5	157.8
	9.07	0.131	43.8	335.7
	9.83	0.067	40.6	607.8
	10.59	0.083	94.3	1140.4
	11.45	0.201	359.3	1788.4
	12.12	0.145	290.8	2001.2
	12.88	0.179	469.2	2627.6
	13.64	0.135	401.5	2964.7
	15.16	0.176	658.3	3749.5
	16.69	0.204	817.4	4008.0
	18.21	0.196	746.0	3815.6
	19.74	0.092	330.4	3599.1
	21.26	0.123	475.8	3880.1
	22.02	0.208	671.4	3230.3
	22.78	0.152	793.5	5230.0
RLBF 0m	0.03	0.067	1.8	27.6
	0.47	0.044	1.3	29.7
	1.02	0.031	2.7	85.5
	1.46	0.025	1.3	51.9
	2.58	0.038	0.9	22.6
	3.19	0.031	3.0	96.7
	4.13	0.075	1.1	14.1
	4.51	0.062	9.3	150.5
	4.95	0.047	39.4	843.9
	5.43	0.046	36.0	791.6
	6.04	0.014	2.2	156.9
	7.07	0.117	1.4	12.4
	7.51	0.081	1.3	16.4
	8.15	0.088	1.8	20.3
	9.08	0.021	0.8	36.6
	10.23	0.020	1.5	77.8
	10.94	0.082	0.9	11.3
	12.10	0.060	1.0	16.0
	13.01	0.113	0.6	5.2
	14.01	0.109	0.6	5.0
	16.03	0.101	0.6	6.3
	18.20	0.106	1.8	16.5
	20.10	0.152	10.5	69.1
RLBF 50m	0.03	0.015	122.6	8348.5
	0.32	0.014	5.3	393.3
	0.59	0.050	1.3	25.9
	0.76	0.059	175.8	2991.1
	1.23	0.016	45.4	2850.3
	1.60	0.015	29.2	1975.8
	2.06	0.010	23.4	2417.6
	2.48	0.016	35.2	2188.8
	3.22	0.076	177.0	2322.5
	4.13	0.077	162.3	2117.9
	4.57	0.100	234.5	2345.9
	5.14	0.028	52.0	1883.0
	6.17	0.126	193.0	1529.0
	7.07	0.040	58.7	1481.7
	8.18	0.033	37.2	1141.1
RFF 0m	0.03	0.211	5.3	25.1
	0.43	0.099	8.7	87.6
	0.98	0.073	1.2	16.4
	1.37	0.132	0.6	4.6
	1.77	0.170	0.5	2.8
	2.16	0.190	0.4	1.9

BD2 denotes measurements below the detection limit of 2 g m-3 in the supernatant measured by potentiometric titration

Table 5. Water content and chloride concentrations of sediment samples in and adjacent to fissures.

Borehole number	Depth (m)	Gravimetric water content ($g\ g^{-1}$)	Chloride ($mg\ Cl\ kg^{-1}$ soil)	Chloride ($g\ Cl\ m^{-3}$ water)
RFF 0m	2.50	0.206	0.3	1.3
	2.90	0.116	1.2	10.1
	3.29	0.140	3.7	26.6
	4.08	0.181	16.3	89.8
	5.04	0.180	40.8	226.9
	6.05	0.163	47.6	291.5
	7.06	0.185	33.8	182.9
	8.20	0.197	45.3	229.8
	9.10	0.172	43.5	252.4
	10.10	0.166	38.2	230.7
	11.02	0.196	42.0	214.5
	12.15	0.129	35.1	273.0
	13.17	0.128	29.6	231.4
	14.16	0.098	13.0	133.5
	16.05	0.142	7.2	50.9
	17.01	0.243	8.9	36.5
	18.14	0.205	6.6	32.3
	19.10	0.203	6.6	32.5
	20.06	0.201	4.8	23.8
	20.85	0.063	1.5	24.7
	21.67	0.162	4.2	26.2
	23.10	0.040	1.5	37.9
	24.63	0.202	1.6	8.0
RFF 10m	0.03	0.224	3.9	17.3
	0.43	0.078	31.1	399.7
	0.82	0.075	160.5	2149.8
	1.28	0.124	369.2	2980.3
	1.68	0.151	268.8	1784.3
	2.07	0.158	176.7	1115.2
	2.47	0.175	178.4	1017.4
	3.02	0.107	88.6	828.5
	3.41	0.090	70.7	788.1
	3.98	0.101	69.9	688.6
	5.17	0.131	69.9	535.0
	6.13	0.159	77.2	486.4
	7.10	0.056	23.8	421.4
	8.09	0.073	27.0	372.2
	9.07	0.174	50.3	289.5
	10.09	0.165	42.3	256.5
	11.02	0.133	29.2	219.6
	12.15	0.077	19.6	255.6
	14.07	0.061	6.5	107.2
	16.00	0.166	5.3	32.2

Borehole number	Depth (m)	Gravimetric water content ($g\ g^{-1}$)	Chloride ($mg\ Cl\ kg^{-1}$ soil)	Chloride ($g\ Cl\ m^{-3}$ water)
RFF 50m	0.03	0.115	1.2	10.8
	0.47	0.082	5.0	60.8
	0.87	0.054	17.2	319.1
	1.33	0.155	102.3	659.3
	1.71	0.172	130.2	756.8
	2.15	0.166	121.6	734.3
	2.56	0.174	124.6	715.4
	3.00	0.084	59.3	704.4
	3.58	0.083	53.6	645.6
	4.16	0.156	82.9	532.9
	4.53	0.179	89.9	501.9
	5.11	0.165	77.4	468.4
	6.05	0.164	74.1	452.5
	6.96	0.153	64.9	425.2
	7.94	0.102	36.2	356.1
	8.92	0.219	71.5	326.4
	10.01	0.155	45.9	296.6
	10.99	0.210	56.4	268.3
	11.96	0.098	25.1	256.0
	13.06	0.057	13.8	243.7

BD2 denotes measurements below the detection limit of 2 g m-3 in the supernatant measured by potentiometric titration

Table 6. Gravitational, water, total (water + gravitational), and osmotic potentials of sediment samples collected beneath and adjacent to fissures.

Borehole number	Depth (m)	Gravitational potential (MPa)	Water potential (MPa)	Total potential (MPa)	Depth (m)	Osmotic potential (MPa)
HBF 0m	0.46	1.47	-15.86	-14.39		
	1.49	1.46	-5.60	-4.14		
	1.92	1.45	-5.34	-3.89		
	3.48	1.44	-1.69	-0.25		
	4.54	1.43	-0.96	0.47		
	6.52	1.41	-0.54	0.87		
	8.38	1.39	-0.21	1.18		
	9.45	1.38	-0.26	1.12		
	11.77	1.36	-0.27	1.09		
	14.81	1.33	-0.45	0.88		
	17.47	1.30	-0.81	0.49		
	18.99	1.28	-0.52	0.76		
	20.51	1.27	-1.04	0.23		
	22.45	1.25	-0.66	0.59		
HBF 10m	0.49	1.47	-17.66	-16.19		
	1.10	1.46	-8.70	-7.24		
	2.10	1.45	-5.72	-4.27		
	4.15	1.43	-4.76	-3.33		
	7.92	1.39	-3.20	-1.81		
	9.45	1.38	-2.34	-0.96		
	11.37	1.36	-1.90	-0.54		
	12.95	1.34	-1.53	-0.19		
	15.09	1.32	-1.65	-0.33		
	17.50	1.30	-1.07	0.23		
	21.24	1.26	-0.69	0.57		
	23.96	1.24	-0.75	0.49		
HBF 50m	0.43	1.47	-15.34	-13.87		
	1.52	1.46	-16.24	-14.78		
	1.98	1.45	-9.71	-8.26		
	3.51	1.44	-7.62	-6.18		
	5.03	1.42	-7.94	-6.52		
	6.10	1.41	-6.93	-5.52		
	7.62	1.40	-4.96	-3.56		
	9.08	1.38	-4.41	-3.03		
	9.88	1.37	-5.82	-4.45		
EFF35 0m	0.23	2.11	-2.28	-0.17	0.29	0.00
	0.53	2.10	-0.58	1.53	0.59	0.00
	0.84	2.10	-0.93	1.17	0.90	0.00
	1.20	2.10	-0.35	1.75	1.26	0.00
	1.51	2.09	-0.37	1.72	1.57	0.00
	1.81	2.09	-0.35	1.74	1.87	0.00
	2.12	2.09	-0.31	1.78	2.18	0.00
	2.52	2.08	-0.33	1.75	2.58	0.00
	2.76	2.08	-0.30	1.78	2.82	0.00
	3.06	2.08	-0.30	1.78	3.12	0.00
	3.37	2.07	-0.31	1.76	3.43	0.00
	3.67	2.07	-0.31	1.76	3.73	0.00
	4.04	2.07	-0.38	1.69	4.10	0.00
	4.31	2.07	-0.36	1.70	4.37	0.00
	4.62	2.06	-0.41	1.66	4.68	0.00
	4.89	2.06	-0.38	1.68	4.95	0.00
	5.35	2.06	-0.45	1.60	5.41	0.00
	5.87	2.05	-0.61	1.44	5.93	-0.03
	6.17	2.05	-0.33	1.72	6.23	0.00
	6.48	2.04	-0.40	1.64	6.54	0.00
	7.03	2.04	-0.88	1.16	7.03	0.00
	7.70	2.03	-0.64	1.39	7.76	0.00
	8.15	2.03	-0.62	1.40	8.15	0.00
	8.67	2.02	-0.54	1.48	8.21	-0.02
	9.10	2.02	-0.81	1.21	8.67	-0.02
	9.71	2.01	-1.60	0.41	9.68	0.00
	10.30	2.01	-1.90	0.10		
	10.70	2.00	-2.72	-0.72		

Table 6. Gravitational, water, total (water + gravitational), and osmotic potentials of sediment samples collected beneath and adjacent to fissures.

Borehole number	Depth (m)	Gravitational potential (MPa)	Water potential (MPa)	Total potential (MPa)	Depth (m)	Osmotic potential (MPa)
EFF35 0m	11.30	2.00	-2.44	-0.45	11.32	-0.66
	11.80	1.99	-2.84	-0.85		
	12.20	1.99	-4.11	-2.12		
	12.80	1.98	-5.04	-3.06		
	13.30	1.98	-4.80	-2.82		
	14.20	1.97	-4.58	-2.62	14.31	-0.64
	14.90	1.96	-5.41	-3.45		
	15.80	1.95	-4.65	-2.70		
	16.50	1.95	-5.00	-3.05		
	17.40	1.94	-4.89	-2.95	17.42	-0.63
	18.00	1.93	-4.89	-2.95		
	18.90	1.92	-4.54	-2.62		
	19.40	1.92	-4.68	-2.76		
	20.40	1.91	-4.32	-2.41	20.47	-0.66
EFF36 10m	0.23	2.11	-11.50	-9.42		
	0.53	2.10	-9.79	-7.68	0.59	-1.00
	0.99	2.10	-9.52	-7.42	1.05	-0.95
	1.30	2.10	-7.77	-5.68	1.36	-0.84
	1.60	2.09	-6.92	-4.82	1.66	-0.79
	1.91	2.09	-7.69	-5.60	1.97	-0.88
	2.21	2.09	-6.22	-4.13	2.27	-0.85
	2.85	2.08	-7.41	-5.33	2.58	-0.85
	3.15	2.08	-7.16	-5.09	3.22	-0.78
	3.46	2.07	-7.14	-5.07	3.52	-0.74
	3.76	2.07	-7.79	-5.72	3.83	-0.61
	4.07	2.07	-8.90	-6.84	4.13	-0.74
	4.40	2.06	-7.49	-5.42	4.47	-0.42
	4.71	2.06	-7.78	-5.72	4.77	-0.73
	5.01	2.06	-7.65	-5.59	5.07	-0.64
	5.96	2.05	-8.41	-6.36	5.47	-0.68
	6.26	2.05	-7.82	-5.77	6.32	-0.65
	6.57	2.04	-6.56	-4.52	6.63	-0.64
	6.87	2.04	-6.73	-4.68		
	7.24	2.04	-6.66	-4.62		
	7.64	2.03	-6.61	-4.58		
	8.15	2.03	-6.35	-4.33	8.21	-0.61
	8.61	2.02	-6.18	-4.16		
	9.19	2.02	-6.95	-4.93		
	9.80	2.01	-7.74	-5.73	9.86	-0.60
	10.30	2.01	-6.69	-4.68		
	10.70	2.00	-6.35	-4.35		
	11.20	2.00	-6.26	-4.26	11.30	-0.43
	11.90	1.99	-5.81	-3.81		
	12.30	1.99	-6.06	-4.07		
	12.80	1.98	-6.08	-4.10	12.80	-0.63
	13.20	1.98	-5.83	-3.85		
	13.70	1.97	-5.81	-3.83		
	14.50	1.97	-5.76	-3.79	14.50	-0.71
	15.40	1.96	-5.74	-3.79		
	16.00	1.95	-5.70	-3.75	16.10	-0.63
	17.00	1.94	-5.59	-3.64		
	17.60	1.94	-5.74	-3.81	17.60	-0.67
	18.50	1.93	-5.18	-3.25		
	19.10	1.92	-5.40	-3.48		
	19.90	1.91	-5.41	-3.49		
	20.80	1.90	-4.90	-2.99	20.90	-0.67
	22.10	1.89	-5.52	-3.63		
	23.50	1.88	-5.12	-3.24	23.80	-0.69
	25.30	1.86	-4.90	-3.04		
	26.80	1.85	-4.88	-3.03	26.90	-0.66
	29.90	1.81	-5.27	-3.46	30.00	-0.75
EFF59 10m	0.27	2.11	-4.87	-2.77	0.22	-0.33
	0.57	2.10	-7.15	-5.05	0.53	-0.89

Table 6. Gravitational, water, total (water + gravitational), and osmotic potentials of sediment samples collected beneath and adjacent to fissures.

Borehole number	Depth (m)	Gravitational potential (MPa)	Water potential (MPa)	Total potential (MPa)	Depth (m)	Osmotic potential (MPa)
EFF59 10m	1.33	2.09	-6.89	-4.79	1.29	-1.01
	1.61	2.09	-7.76	-5.67	1.56	-0.93
	1.94	2.09	-6.68	-4.60	1.90	-0.93
	2.25	2.09	-7.88	-5.79	2.20	-0.92
	2.89	2.08	-6.13	-4.05	2.84	-0.86
	3.19	2.08	-6.15	-4.08	3.15	-0.82
	3.50	2.07	-6.90	-4.82	3.45	-0.80
	3.80	2.07	-6.51	-4.44	3.76	-0.83
	4.12	2.07	-9.41	-7.34	4.06	-0.81
	4.63	2.06	-7.01	-4.95	4.58	-0.56
	4.93	2.06	-6.86	-4.80	4.88	-0.74
	5.24	2.06	-5.82	-3.76	5.19	-0.73
	6.00	2.05	-5.58	-3.53	5.95	-0.65
	6.30	2.05	-6.11	-4.07	6.26	-0.65
	6.61	2.04	-6.16	-4.11	6.56	-0.63
	6.91	2.04	-5.74	-3.70	6.87	-0.64
	7.17	2.04	-7.65	-5.61	6.96	-0.66
	7.55	2.03	-5.70	-3.66	7.51	-0.62
	7.95	2.03	-5.72	-3.69	7.90	-0.65
	8.25	2.03	-6.11	-4.08	8.21	-0.67
	9.81	2.01	-5.67	-3.65	9.76	-0.65
	11.20	2.00	-5.57	-3.57	11.10	-0.68
	11.90	1.99	-5.93	-3.94	11.80	-0.74
	12.70	1.98	-5.47	-3.49	12.70	-0.70
	14.30	1.97	-5.35	-3.38	14.20	-0.70
	15.80	1.95	-5.47	-3.52	15.80	-0.42
	17.40	1.94	-4.91	-2.97	17.40	-1.11
	19.00	1.92	-5.18	-3.26	18.90	-0.70
	20.50	1.91	-4.86	-2.95	20.50	-0.74
	22.10	1.89	-5.08	-3.19	22.00	-0.69
	23.60	1.88	-4.93	-3.06	23.60	-0.73
	25.30	1.86	-4.93	-3.07	25.20	-0.71
EFF88 0m	0.27	2.11	-3.03	-0.92	0.22	-0.02
	0.57	2.10	-2.90	-0.80	0.53	0.00
	1.15	2.10	-2.00	0.10	1.10	0.00
	1.46	2.09	-1.30	0.80	1.41	0.00
	1.76	2.09	-0.80	1.29	1.71	0.00
	2.07	2.09	-0.73	1.35	2.02	0.00
	2.39	2.08	-0.75	1.33	2.34	-0.04
	2.71	2.08	-0.64	1.45	2.66	-0.09
	3.01	2.08	-0.63	1.45	2.96	-0.06
	3.32	2.08	-0.63	1.44		
	3.62	2.07	-0.75	1.32	3.57	-0.10
	3.92	2.07	-1.11	0.96	3.89	-0.09
	4.26	2.07	-0.85	1.21	4.21	-0.10
	4.56	2.06	-0.62	1.45	4.52	-0.07
	4.87	2.06	-0.40	1.66	4.82	-0.03
	5.17	2.06	-0.54	1.52	5.13	0.00
	5.81	2.05	-0.59	1.47	5.77	-0.08
	6.33	2.05	-1.23	0.82	6.29	-0.28
	7.05	2.04	-1.84	0.20	7.06	-0.32
	7.89	2.03	-1.61	0.43	7.84	-0.53
	8.63	2.02	-2.79	-0.77	8.59	-0.54
	9.20	2.02	-3.32	-1.30	9.15	-0.49
	9.78	2.01	-3.06	-1.05	9.73	-0.49
	10.70	2.00	-2.86	-0.85	10.90	-0.53
	11.70	1.99	-3.74	-1.75	11.70	-0.60
	12.60	1.98	**-3.79**	-1.81	12.50	-0.54
EFF92 0m	0.27	2.11	-11.85	-9.75		
	0.59	2.10	-10.50	-8.39	0.46	0.00
	1.35	2.09	-5.94	-3.85	1.40	-0.19
	1.96	2.09	-1.65	0.44	2.01	-0.23
	3.18	2.08	-2.17	-0.09	3.23	-0.26

Table 6. Gravitational, water, total (water + gravitational), and osmotic potentials of sediment samples collected beneath and adjacent to fissures.

Borehole number	Depth (m)	Gravitational potential (MPa)	Water potential (MPa)	Total potential (MPa)	Depth (m)	Osmotic potential (MPa)
EFF92 0m	4.40	2.06	-1.15	0.91	4.27	-0.12
	5.92	2.05	-1.02	1.03	5.80	-0.19
	6.53	2.04	-1.55	0.50	6.41	-0.25
	7.38	2.04	-1.75	0.28	7.44	-0.41
	9.21	2.02	-2.29	-0.27	8.96	-0.51
	10.43	2.01	-2.66	-0.66	10.61	-0.52
	11.65	1.99	-3.41	-1.42	11.53	-0.53
	12.87	1.98	-3.89	-1.90	12.92	-0.57
	14.03	1.97	-3.86	-1.89	14.21	-0.56
	14.75	1.96	-3.89	-1.92	14.51	-0.57
	15.96	1.95	-3.82	-1.87	15.42	-0.55
EFF96 10m	0.15	2.11	-27.43	-25.32	0.26	-0.01
	0.76	2.10	-13.34	-11.24	0.64	-0.54
	1.62	2.09	-8.53	-6.44	1.72	-0.83
	2.41	2.08	-7.73	-5.65	2.33	-0.75
	3.54	2.07	-8.18	-6.10	3.63	-0.70
	5.12	2.06	-7.23	-5.17	5.23	-0.61
	6.65	2.04	-6.31	-4.27	6.54	-0.58
	8.05	2.03	-6.33	-4.30	7.79	-0.56
	9.69	2.01	-5.75	-3.73	9.19	-0.60
	11.13	2.00	-6.69	-4.69	11.22	-0.60
	12.50	1.99	-5.75	-3.77	12.41	-0.60
	14.02	1.97	-5.17	-3.20	14.11	-0.62
	15.55	1.96	-5.66	-3.71	15.45	-0.62
	16.89	1.94	-5.20	-3.25	16.67	-0.62
EFF119 10m	0.12	2.11	-11.44	-9.34	0.21	-0.01
	0.49	2.10	-9.79	-7.68	0.40	-0.14
	0.85	2.10	-9.36	-7.26	0.76	-0.66
	1.37	2.09	-6.68	-4.59	1.28	-0.66
	1.92	2.09	-8.05	-5.96	2.01	-0.70
	2.29	2.09	-6.76	-4.67	2.38	-0.73
	2.90	2.08	-5.87	-3.79	2.99	-0.72
	3.44	2.07	-6.13	-4.05	3.35	-0.72
	3.99	2.07	-5.66	-3.59	4.08	-0.68
	4.60	2.06	-6.47	-4.41	4.69	-0.67
	5.33	2.06	-5.96	-3.90	5.61	-0.62
	6.13	2.05	-9.29	-7.24	6.40	-0.57
	6.86	2.04	-6.12	-4.08		
	7.65	2.03	-5.29	-3.26		
	8.38	2.03	-4.95	-2.93	8.29	-0.55
	9.17	2.02	-4.72	-2.70		
	9.91	2.01	-5.40	-3.39	10.97	-0.57
	10.70	2.00	-4.59	-2.59		
	12.47	1.99	-4.38	-2.39	12.37	-0.59
	14.30	1.97	-4.25	-2.28	13.29	-0.63
	15.33	1.96	-3.96	-2.01	15.12	-0.59
	17.04	1.94	-4.26	-2.32	16.95	-0.62
	18.87	1.92	-4.32	-2.40	18.78	-0.62
	20.09	1.91	-4.31	-2.40	19.99	-0.65
EFF120 0m	0.09	2.11	-1.41	0.69	0.02	-0.02
	0.55	2.10	-0.64	1.46	0.62	0.00
	1.07	2.10	-0.32	1.78	0.99	0.00
	1.51	2.09	-0.60	1.50	1.60	0.00
	1.98	2.09	-0.57	1.52	1.91	0.00
	2.41	2.08	-0.56	1.53	2.21	0.00
	3.05	2.08	-0.64	1.44	2.97	0.00
	3.81	2.07	-1.06	1.01	3.73	0.00
	3.93	2.07	-0.80	1.27		
	4.57	2.06	-0.55	1.52	4.50	0.00
	5.33	2.06	-0.59	1.47	5.26	0.00
	6.10	2.05	-0.57	1.48	6.02	0.00
	6.98	2.04	-0.65	1.39	6.78	0.00
	7.74	2.03	-0.70	1.33	7.54	0.00

Table 6. Gravitational, water, total (water + gravitational), and osmotic potentials of sediment samples collected beneath and adjacent to fissures.

Borehole number	Depth (m)	Gravitational potential (MPa)	Water potential (MPa)	Total potential (MPa)	Depth (m)	Osmotic potential (MPa)
EFF120 0m	9.14	2.02	-1.01	1.01	9.07	-0.04
	9.91	2.01	-1.17	0.84	9.83	-0.08
	10.79	2.00	-1.15	0.85	10.59	-0.15
	12.19	1.99	-1.40	0.59	12.12	-0.26
	13.72	1.97	-1.80	0.17	13.64	-0.38
	15.24	1.96	-1.66	0.30	15.16	-0.47
	16.76	1.94	-1.99	-0.05	16.69	-0.50
	18.29	1.93	-2.04	-0.11	18.21	-0.48
	19.93	1.91	-2.55	-0.64	19.74	-0.46
	22.86	1.88	-3.05	-1.17	22.78	-0.65
RLBF 0m	0.15	1.05	-0.33	0.72	0.03	0.00
	0.37	1.05	-6.70	-5.65	0.47	0.00
	0.91	1.04	-5.12	-4.08	1.02	-0.01
	2.47	1.02	-2.56	-1.54	2.58	0.00
	4.02	1.01	-4.65	-3.64	4.13	0.00
	5.76	0.99	-3.39	-2.40	5.43	-0.10
	7.41	0.98	-2.19	-1.21	7.51	0.00
	9.63	0.95	-2.47	-1.52		
	10.85	0.94	-2.01	-1.07	10.94	0.00
	12.92	0.92	-1.97	-1.05		
	14.36	0.91	-1.82	-0.91	14.01	0.00
	15.21	0.90	-1.69	-0.79		
	17.47	0.88	-1.81	-0.93		
	19.05	0.86	-1.71	-0.85		
	20.45	0.85	-1.60	-0.75	20.10	-0.01
RLBF 50m	0.67	1.04	-7.17	-6.13	0.59	0.00
	1.68	1.03	-7.02	-5.99	1.60	-0.26
	3.29	1.02	-5.36	-4.34	3.22	-0.30
	4.48	1.01	-5.91	-4.90	4.57	-0.30
	6.25	0.99	-5.19	-4.20	6.17	-0.20
	7.53	0.98	-4.77	-3.79		
RFF 0m	0.37	0.83	-5.86	-5.03	0.43	-0.01
	1.31	0.82	-3.37	-2.55	1.37	0.00
	2.10	0.81	-2.13	-1.32	2.16	0.00
	3.23	0.80	-1.72	-0.92	3.29	0.00
	4.82	0.79	-1.07	-0.28	5.04	-0.03
	5.82	0.78	-1.00	-0.22	6.05	-0.04
	7.35	0.76	-1.08	-0.32	7.06	-0.02
	8.93	0.75	-0.47	0.28	9.10	-0.03
	10.39	0.73	-0.50	0.23	10.10	-0.03
	11.92	0.72	-0.27	0.45	12.15	-0.04
	13.53	0.70	-0.31	0.39	13.17	-0.03
	15.03	0.69	-0.26	0.43		
	16.95	0.67	-1.15	-0.48	17.01	0.00
	18.47	0.65	-1.24	-0.59	18.14	0.00
	19.99	0.64	-1.24	-0.60	20.06	0.00
	21.21	0.63	-1.11	-0.48	21.67	0.00
	23.04	0.61	-0.98	-0.37	23.10	-0.01
	24.96	0.59	-1.39	-0.80	24.63	0.00
RFF 10m	0.37	0.83	-10.39	-9.56	0.43	-0.05
	0.76	0.83	-8.33	-7.50	0.82	-0.28
	1.62	0.82	-5.18	-4.36	1.68	-0.23
	2.41	0.81	-4.07	-3.26	2.47	-0.13
	3.75	0.80	-3.29	-2.49	3.98	-0.09
	4.94	0.78	-3.10	-2.32	5.17	-0.07
	6.46	0.77	-3.09	-2.32	6.13	-0.06
	7.86	0.76	-2.76	-2.00	8.09	-0.05
	9.24	0.74	-2.34	-1.60	9.07	-0.04
	10.39	0.73	-2.20	-1.47	10.09	-0.03
	11.92	0.72	-2.04	-1.32	12.15	-0.03
	13.44	0.70	-1.88	-1.18	14.07	-0.01
	15.15	0.68	-1.84	-1.16		
	16.34	0.67	-2.01	-1.34	16.00	0.00

Table 6. Gravitational, water, total (water + gravitational), and osmotic potentials of sediment samples collected beneath and adjacent to fissures.

Borehole number	Depth (m)	Gravitational potential (MPa)	Water potential (MPa)	Total potential (MPa)	Depth (m)	Osmotic potential (MPa)
RFF 50m	0.15	0.83	-4.12	-3.29	0.03	0.00
	0.76	0.83	-9.36	-8.53	0.87	-0.04
	1.22	0.82	-3.43	-2.61	1.33	-0.09
	1.62	0.82	-4.30	-3.48	1.71	-0.10
	2.44	0.81	-3.06	-2.25	2.56	-0.09
	2.91	0.80	-3.13	-2.33	3.00	-0.09
	3.49	0.80	-2.73	-1.93	3.58	-0.09
	4.07	0.79	-2.77	-1.98	4.16	-0.07
	4.62	0.79	-2.58	-1.79	4.53	-0.07
	5.41	0.78	-2.57	-1.79	5.11	-0.06
	6.51	0.77	-2.23	-1.46	6.05	-0.06
	7.03	0.76	-2.42	-1.66	6.96	-0.06
	8.03	0.75	-2.21	-1.46	7.94	-0.05
	9.01	0.75	-2.11	-1.37	8.92	-0.04
	10.10	0.73	-2.34	-1.61	10.01	-0.04
	11.45	0.72	-2.09	-1.37	11.96	-0.03
	13.14	0.70	-2.53	-1.83	13.06	-0.03

Table 7. Water potentials measured with the filter paper method and the Decagon SC10A thermocouple psychrometer on samples taken from trench beneath Eagle Flat fissure.

Distance (m) from surface depression	Depth (m)	Location	Water potential (MPa) (filter paper)	Water potential (MPa) (Decagon)
0.6	0.3	in fracture fill	-0.02	-0.12
0.3	0.3		-0.02	-0.06
0	0.2		-0.01	0.03
0	0.6		-0.01	-0.05
0	1		-0.01	0.01
-0.3	0.3	adjacent to fracture	-0.16	-0.18
-0.6	0.3		-0.20	-0.20

Table 8. Predawn plant water potentials measured in creosote bushes in the Hueco Bolson and mesquite trees in all other fissures and at distances of 100 m (Eagle Flat) and 50 m from all other fissures.

	Fissure	Outside the fissure	Fissure	Outside the fissure	Fissure	Outside the fissure	Fissure	Outside the fissure	Fissure	Outside the fissure	Fissure	Outside the fissure
Hueco Bolson	13-Oct-94		16-Nov-94		20-Jan-95		14-May-95		22-Jul-95		8-Oct-95	
	-3.21	-5.30	-2.65	-4.23	-2.75	-3.67	-3.16	-5.41	-1.30	-2.60	-3.20	-5.50
	-3.21	-5.30	-3.52	-4.23	-2.96	-3.57	-3.11	-5.41	-1.15	-2.60	-3.50	-5.05
	-2.75	-5.41		-4.03	-2.96	-4.18		-7.14	-1.10	-1.20	-2.80	-5.40
	-2.75	-5.05			-3.11	-7.14			-1.15	-1.50	-2.50	-5.00
	-3.42	-5.05							-0.95	-1.55	-3.40	-5.10
	-3.42	-4.23							-1.00	-13.50	-2.90	-4.90
	-3.52											
	-3.37											
mean	-3.21	-5.06	-3.09	-4.17	-2.95	-4.64	-3.14	-5.98	-1.11	-3.83	-3.05	-5.16
Eagle Flat	14-Oct-94		18-Nov-94		19-Jan-95		12-May-95		20-Jul-95		6-Oct-95	
	-1.22	-2.19	-1.12	-2.81	-0.82	-1.22	-1.43	-2.35	-1.00	-1.70	-0.70	-1.80
	-1.02	-2.60	-1.48	-3.06	-1.73	-1.12	-0.92	-2.35	-0.60	-2.15	-1.00	-1.45
	-1.53	-2.70	-2.24	-2.35	-0.82	-1.33	-1.94	-2.24	-1.20	-1.50	-0.85	-1.95
	-1.02	-2.04	-2.19	-2.55	-3.47		-2.35	-1.99	-1.05	-1.95	-2.60	-1.70
	-1.22	-1.79	-1.33	-2.04	-7.14		-1.07	-2.24	-1.80	-1.60	-2.80	-1.55
	-1.53	-1.79	-1.48				-0.92	-2.35	-2.30	-1.60	-1.15	-1.15
	-1.02	-1.48	-2.91				-0.87		-1.15	-1.90	-0.85	
	-1.53	-3.11	-2.24				-0.66		-1.30	-1.75	-0.95	
	-2.04	-2.24	-2.55				-1.48		-1.05		-1.15	
	-2.24						-1.58		-1.40			
	-1.84											
	-1.02											
	-3.57											
	-4.59											
	-2.30											
	-1.99											
	-1.79											
mean	-1.85	-2.22	-1.95	-2.56	-2.79	-1.22	-1.32	-2.25	-1.29	-1.77	-1.34	-1.60
Red Light	11-Oct-94		17-Nov-94		20-Jun-95							
Bolson	-2.30	-1.63	-3.62	-2.81	-2.96	-1.48						
	-1.63	-1.53	-3.72	-2.65	-2.96	-1.43						
	-1.73	-1.58	-2.24	-2.24	-2.65	-1.63						
	-1.73	-1.89		-2.35	-2.65	-1.43						
	-1.94	-2.04										
	-1.22	-3.06										
	-1.84	-1.58										
	-1.84	-2.04										
		-1.92										
mean	-1.78		-3.20	-2.51	-2.81	-1.49						
Ryan Flat	12-Oct-94		18-Nov-94		19-Jan-95		13-May-95		23-Jul-95		8-Oct-95	
	-1.22	-3.42	-1.28	-3.21	-1.63	-6.32	-1.02	-3.47	-1.05	-3.05	-1.40	-3.05
	-1.22	-3.26	-1.43	-3.77	-1.22		-1.53	-3.47	-1.20	-3.35	-1.30	-3.10

Table 8. Predawn plant water potentials measured in creosote bushes in the Hueco Bolson and mesquite trees in all other fissures and at distances of 100 m (Eagle Flat) and 50 m from all other fissures.

Ryan Flat	-1.33	-3.88	-1.73	-4.13	-1.58	-4.59	-1.28	-3.37	-1.30	-2.90	-0.50	-2.70
	-1.99	-3.88	-1.84	-4.08	-1.63	-3.57	-1.33	-2.96	-1.50	-2.90	-0.60	-2.60
	-1.73	-3.26	-1.84	-3.21	-1.68	-3.47	-1.63		-1.75	-3.50	-1.45	-2.75
	-1.79	-3.32	-1.89	-2.96	-1.43		-1.38		-1.50	-3.15	-1.60	-2.25
	-1.79	-3.21	-1.68	-3.57	-1.84		-1.53		-1.35	-3.60	-1.65	-2.65
	-2.04		-2.24	-3.26	-1.73		-1.17		-1.15	-3.20	-1.15	-2.55
	-1.94		-1.84	-3.11			-1.17		-2.75		-0.95	
	-0.97		-2.55				-1.53		-3.00		-0.85	
	-1.07		-2.75				-2.55				-1.00	
	-1.84		-3.11				-1.43					
	-1.99											
	-1.58											
	-1.68											
mean	-1.61	-3.46	-2.01	-3.48	-1.59	-4.49	-1.46	-3.32	-1.66	-3.21	-1.13	-2.71

Table 9. Chloride concentrations (g m^{-3}) in sediment samples collected in the trench beneath Eagle Flat fissure.

		Distance (m) from the center of the surface fissure																		
		-1.5	-1.2	-0.9	-0.6	-0.3	0	0.3	0.4	0.6	0.8	0.9	1	1.2	1.4	1.5	1.6	1.8	2.1	2.4
Depth (m)	0.3	255	46	24	39	20	50	32		113		97		42		316		371	149	308
	0.6	3929	788	185	25	19	22	19		164		983		616		420		314	4260	811
	0.9	6708	2289	597	83	17	12	28		127		341		221		10541		147	7567	240
	1.2	5937	3320	652	101	18	20	23		112		68		46		14548		207	469	4260
	2		7726		5344		577			46				25				226		679
	2.3		6449		4542		234			25				13				137		579
	2.6				1775		168			18				23				166		
	3.41				1775		168			18				23				166		
	3.71				1364		174			25				13				16		
	4.01				1660		340			916				24				21		
	4.56						171		11		12		17	6	16		8			
	4.76								8				4	10	10		4			
	4.96								3		3		9	3	8					
	5.16								5		4		4	5	2		6			
	5.36								5		4		6	4	6		5			
	5.56								7		12		11	7	7					

Table 10. Chlorine-36, tritium, deuterium, and oxygen-18 ratios in samples collected beneath and adjacent to fissures.

Borehole	Chlorine-36		Tritium		Stable isotopes		
number	Depth interval (m)	$^{36}Cl/Cl \times 10^{15}$	Depth interval (m)	Tritium (TU)	Depth interval (m)	$\delta^{18}O$	$\delta^{2}D$
HBF 0m	14.8-16.3	448 ± 29	0.1-1.3	17.5 ± 0.8	1.3-1.5	-6.3	-49
			4.2-4.9	13.8 ± 0.7	1.3-1.5	-6.2	-50
			10.1-10.4	9.3 ± 0.7	2.7-2.8	-7.8	-57
			13.9-14.2	21.7 ± 0.7	8.9-9.0	-7.3	-49
			17.2-17.4	5.2 ± 0.4	8.9-9.0	-7.0	-48
					13.5-13.6	-7.8	-58
					22.6-22.7	-7.5	-57
HBF 10m			0.0-0.9	37.8 ± 1.1			
			2.9-4.9	31.7 ± 0.9			
			9.9-10.4	42.2 ± 0.9			
			20.2-20.4	5.9 ± 0.4			
			25.7-26.4	10.9 ± 0.8			
HBF 50m	7.4-7.6	434 ± 29	3.8-4.2	56.4 ± 1.1	0.1-0.2	7.1	-17
			7.3-8.1	14.6 ± 0.5	1.2-1.3	-2.3	-45
					4.2-4.4	-2.7	-45
					8.3-8.4	-3.9	-47
					8.3-8.4	-4.3	-49
					9.9-10.0	-4.2	-49
EFF92 0m	1.5-1.6	399 ± 30	1.4-1.83	24.4 ± 0.9	0.1-0.2	0.9	-36
	4.6-4.9	383 ± 29	4.5-4.9	33.2 ± 1.1	3.9-4.0	-5.4	-49
			10.2-10.8	7.9 ± 0.5	8.5-8.6	-3.6	-45
			15.2-15.8	6.8 ± 0.4	22.0-22.1	-4.1	-50
			20.2-20.5	17.7 ± 0.6			
EFF36 10m	2.9-3.1	375 ± 30					
	6.5-6.7	438 ± 29					
	13.9-14.1	390 ± 30					
	22.0-22.1	284 ± 29					
	28.2-28.5	291 ± 29					
	30.2-30.4	462 ± 29					
EFF96 10m			5.2-7.2	26.3 ± 0.7	0.3-0.5	1.1	-39
			10.0-10.8	14.1 ± 0.7	0.5-0.6	-0.4	-39
			14.9-15.4	10.8 ± 0.5	4.6-4.9	-1.8	-42
					7.8-8.0	-2.6	-46
					16.3-16.4	-3.7	-50
RFF 0m	5.9-6.4	546 ± 30	0.1-0.2	17.2 ± 1.2	3.5-3.6	-3.6	-44
	9.8-9.9	527 ± 30	2.5-2.7	7.8 ± 0.9	6.5-6.6	-4.8	-49
	13.8-14.3	651 ± 43	6.1-6.2	15.5 ± 1.4	9.5-9.6	-4.4	-49
			11.0-11.2	6.1 ± 0.9	12.6-12.7	-5.4	-51
			17.2-17.3	7.4 ± 0.7	18.8-18.9	-6.0	-56
			20.1-20.2	3.8 ± 0.9	24.8-24.9	-6.9	-58
			25.2-25.3	4.3 ± 0.8	24.8-24.9	-6.9	-58
RFF 10m	5.0-5.3	550 ± 31					
	10.2-10.6	537 ± 31					
RFF 50m			4.9-5.7	34.5 ± 0.8	0.3-0.5	-1.2	-43
			7.2-7.7	13.6 ± 0.6	3.0-3.2	-2.5	-43
			10.3-10.8	13.4 ± 0.5	6.1-6.2	-3.2	-44
					9.1-9.2	-3.9	-47
					12.2-12.3	-4.4	-48
RLB 0m	4.5-4.9	713 ± 32			2.6-2.7	-7.9	-63
					5.5-7.2	-5.7	-50
					8.5-8.7	-6.8	-53
					11.6-11.8	-7.1	-54
					14.6-14.8	-7.5	-54
					20.5-20.6	-7.5	-55
RLB 50m					1.1-1.3	1.2	-36
					2.7-2.9	-2.0	-43
					4.9-5.1	-3.1	-46
					8.4-8.6	-3.9	-46

Table 11. Apparent electrical conductivity measured with EM31 and EM38 in vertical and horizontal dipole modes along transects perpendicular to the trends of the fissures.

Hueco Bolson			Eagle Flat (transect 1)			Eagle Flat (transect 2)			Red Light Bolson (transect 1)		
	3/28/94	3/28/94		3/29/94	3/29/94		3/29/94	3/29/94		8/20/94	8/20/94
Distance (m)	EC_a VD mS m^{-1}	EC_a HD mS m^{-1}	Distance (m)	EC_a VD mS m^{-1}	EC_a HD mS m^{-1}	Distance (m)	EC_a VD mS m^{-1}	EC_a HD mS m^{-1}	Distance (m)	EC_a VD mS m^{-1}	EC_a HD mS m^{-1}
	EM31	EM31		EM31	EM31		EM31	EM31		EM31	EM31
-100	11.7	10.1	-100	66	44	-100	43	29	0	0	7
-95	12.2	9.8	-95	71	53	-95	44	31	1	1	8
-90	11.5	9.6	-90	70	47	-90	44	32	2	8	0
-85	11.9	9.6	-85	62	40	-85	46	29	3	9	0
-80	12.1	9.4	-80	52	36	-80	45	30	4	10	1
-75	12.3	10.1	-75	50	37	-75	45	30	5	10	0
-70	12.7	10.3	-70	48	32	-70	47	31	6	10	1
-65	12.7	10.5	-65	44	33	-65	50	33	7	10	1
-60	12.6	11	-60	46	33	-60	54	40	8	10	1
-55	13.6	10.2	-55	45	33	-55	56	37	9	10	3
-50	13.4	10.5	-50	45	32	-50	56	37	10	10	1
-45	14.6	11.4	-45	46	31	-45	60	36	20	9	2
-40	15.4	12.4	-40	48	33	-40	63	45	30	9	1
-35	15	11.7	-35	49	33	-35	63	43	40	9	2
-30	16.3	12.1	-30	51	35	-30	60	40	50	10	3
-25	16.2	12.3	-25	51	37	-25	63	40	60	8	2
-20	17.3	12	-20	52	36	-20	69	51	70	8	2
-15	16.8	12.9	-15	50	35	-15	76	53	80	8	2
-10	15.5	12.2	-10	59	36	-10	76	52	90	8	2
-9	15.5	11.6	-9	59	38	-9	75	51	100	8	1
-8	16	11.4	-8	62	41	-8	74	50			
-7	15.2	10.7	-7	67	42	-7	71	50			
-6	14.6	10.7	-6	71	42	-6	68	50			
-5	14.4	10.3	-5	75	45	-5	67	50			
-4	14.5	10.6	-4	76	48	-4	66	50			
-3	14.2	10.1	-3	76	57	-3	68	51			
-2	14.6	9.3	-2	76	60	-2	72	48			
-1	14.4	9.8	-1	76	62	-1	77	45			
0	14	10.4	0	80	64	0	79	47			
1	14.6	9.6	1	79	63	1	78	51			
2	14.5	10.3	2	78	65	2	78	53			
3	14.2	10.3	3	79	59	3	78	54			
4	14.1	10.1	4	78	52	4	76	55			
5	14.4	10.3	5	76	50	5	75	53			
6	14.3	9.7	6	74	46	6	76	50			
7	14.3	10.1	7	69	44	7	76	48			
8	13.8	10.3	8	67	41	8	76	47			
9	13.3	10	9	65	40	9	72	48			
10	13.3	9.6	10	62	38	10	70	49			
15	13.6	10.5	15	53	36	15	64	44			
20	12	9.6	20	47	34	20	65	38			
25	12.1	8.9	25	45	29	25	56	40			
30	11.7	9.4	30	43	28	35	52	37			
35	11.2	8.9	35	42	28	40	53	36			
40	10.6	8.4	40	41	29	45	53	34			
45	11.7	8.3	45	41	28	50	54	38			
50	10.4	10	50	42	31	50	54	38			
55	13	9.2	55	43	31	55	58	38			
60	12.3	10.5	60	45	32	60	59	39			
65	12.7	11.1	65	46	32	65	56	41			
70	13.1	10.8	70	45	30	70	56	38			
75	14.3	11	75	42	28	75	50	31			
80	12.7	11.3	80	41	29	80	43	28			
85	12.7	10.2	85	42	28	85	43	27			
90	13.1	10.5	90	45	32	90	46	31			
95	13.7	10.9	95	50	37	95	48	34			
100	14.3	11.1	100	51	38	100	50	36			

Table 11. Apparent electrical conductivity measured with EM31 and EM38 in vertical and horizontal dipole modes along transects perpendicular to the trends of the fissures.

Red Light Bolson (transect 2)			Ryan Flat			Ryan Flat		
	3/30/94	3/30/94		8/21/94	8/21/94		8/21/94	8/21/94
Distance (m)	EC_a VD mS m^{-1}	EC_a HD mS m^{-1}	Distance (m)	EC_a VD mS m^{-1}	EC_a HD mS m^{-1}	Distance (m)	EC_a VD mS m^{-1}	EC_a HD mS m^{-1}
	EM31	EM31		EM31	EM31		EM38	EM38
-100	16	11	-100	29	24	-100	21.8	15
-95	17	10	-95	30	23	-95	18.7	11
-90	17	10	-90	31	24	-90	20.3	11
-85	16	10	-85	32	23	-85	22.1	11
-80	17	10	-80	32	24	-80	22.7	13
-75	17	10	-75	31	23	-75	22.2	12
-70	17	10	-70	30	24	-70	22.1	14
-65	17	10	-65	28	22	-65	21.8	13
-60	17	10	-60	28	22	-60	20.6	10
-55	17	10	-55	30	23	-55	19.4	11
-50	18	11	-50	33	23	-50	21.3	11
-45	19	11	-45	33	24	-45	20.9	10
-40	19	11	-40	32	24	-40	21.3	12
-35	19	12	-35	32	24	-35	19.4	11
-30	20	12	-30	31	23	-30	19.8	12
-25	23	14	-25	32	23	-25	18	10
-20	27	15	-20	35	25	-20	18.5	9
-15	30	19	-15	35	28	-15	20.7	16
-10	34	21	-10	45	31	-10	25.5	15
-9	36	21	-9	47	32	-9	26	15
-8	37	21	-8	50	34	-8	26.2	17
-7	36	20	-7	54	33	-7	28.8	17
-6	38	22	-6	55	40	-6	29.6	19
-5	39	20	-5	51	53	-5	31.1	27
-4	39	22	-4	49	57	-4	35.4	27
-3	37	22	-3	50	57	-3	19.2	32
-2	38	23	0	54	39	0	25.9	17
-1	36	22	1	53	38	1	23.8	17
0	38	21	2	51	39	2	23	16
1	37	22	3	51	38	3		17
2	34	23	4	51	38	4	19.5	15
3	35	22	5	50	34	5	19.5	14
4	34	22	6	48	30	6	20	13
5	34	20	7	46	29	7	19	12
6	32	20	8	45	28	8	18.9	12
7	29	18	9	44	27	9	18	12
8	29	18	10	43	27	10	18.6	13
9	29	20	15	38	25	15	17.3	12
10	28	18	20	37	25	20	15.9	12
15	22	14	25	37	26	25	16.1	11
20	19	11	30	39	27	30	17	12
25	18	13	35	41	28	35	18.7	11
30	17	11	40	41	28	40	18.9	14
35	17	11	45	46	30	45	18.4	13
40	18	13						
45	20	13						
50	19	12						
55	19	12						
60	19	12						
65	20	14						
70	20	13						
75	21	15						

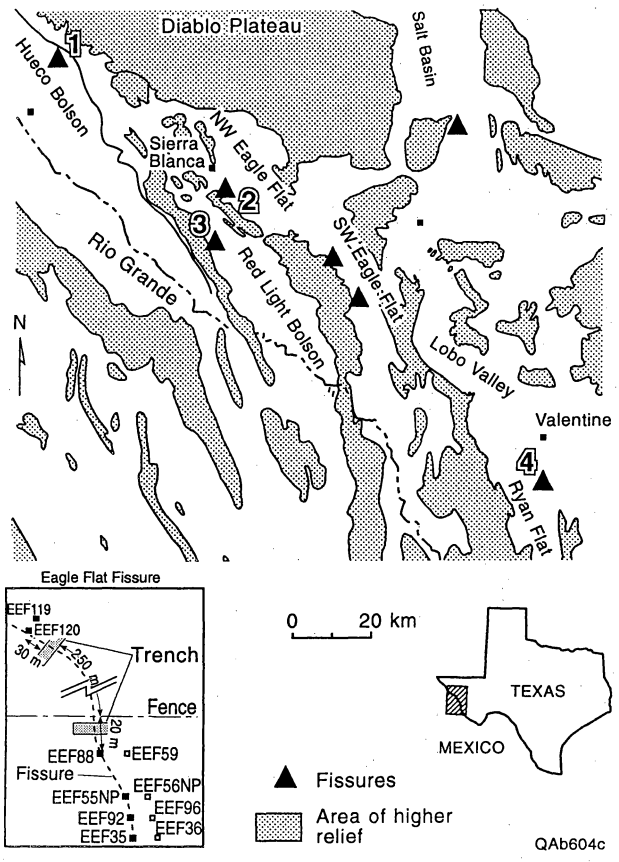
Diablo Plateau
Salt Basin
Hueco Bolson
1
Sierra Blanca
NW Eagle Flat
2
3
Rio Grande
Red Light Bolson
SW Eagle Flat
Lobo Valley
N
Valentine
4
Ryan Flat
Eagle Flat Fissure
EEF119
EEF120
30 m
250 m
Trench
Fence
20 m
EEF88
EEF59
Fissure
EEF56NP
EEF55NP
EEF96
EEF92
EEF36
EEF35
0
20 km
TEXAS
MEXICO
Fissures
Area of higher relief
QAb604c

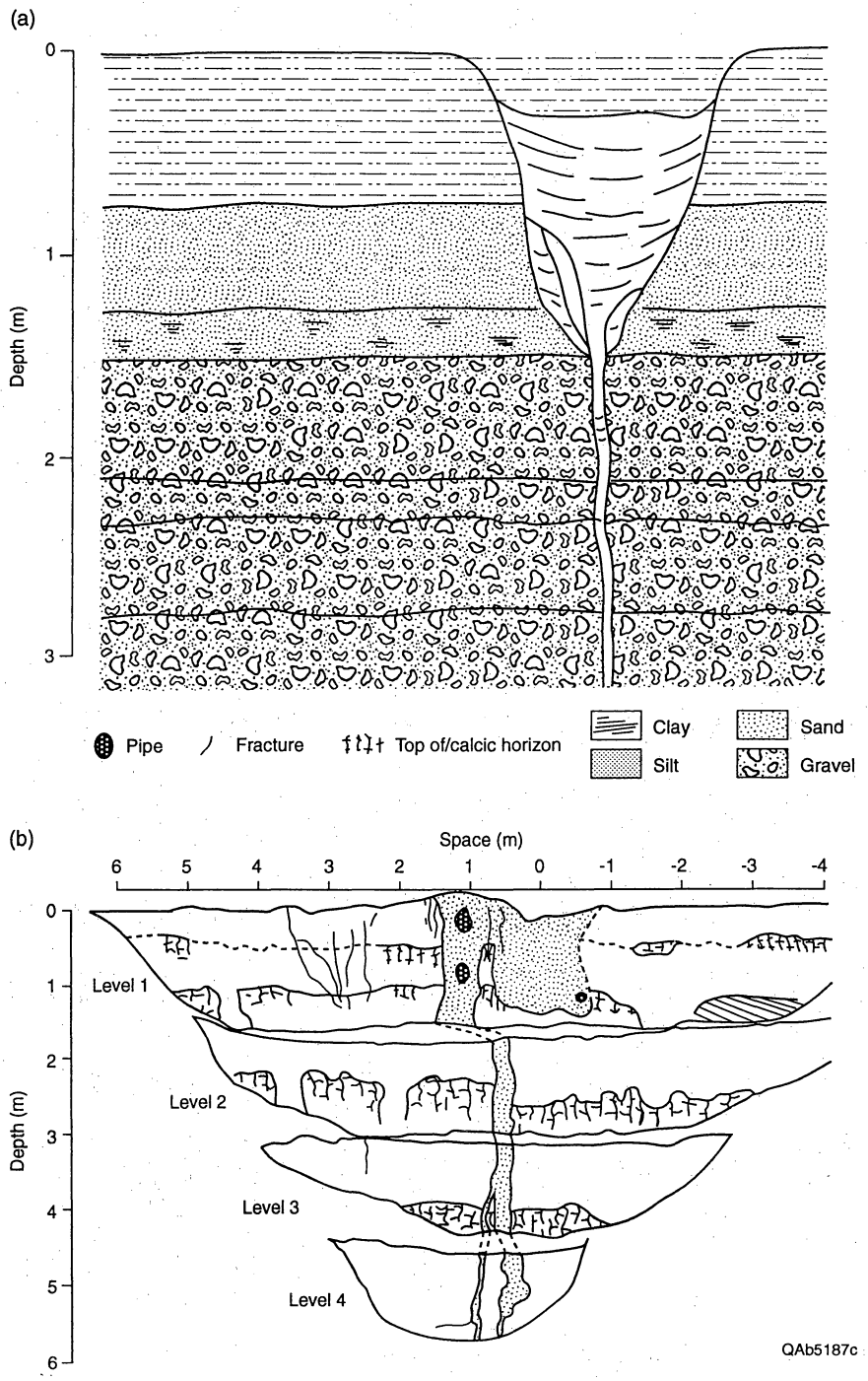
(a)
Depth (m)
0
1
2
3
Pipe
Fracture
Top of/calcic horizon
Clay
Silt
Sand
Gravel
(b)
Space (m)
6
5
4
3
2
1
0
-1
-2
-3
-4
Depth (m)
0
1
2
3
4
5
6
Level 1
Level 2
Level 3
Level 4
QAb5187c


Road
Fissure
Fence
0
1/2 km
QAb6205c

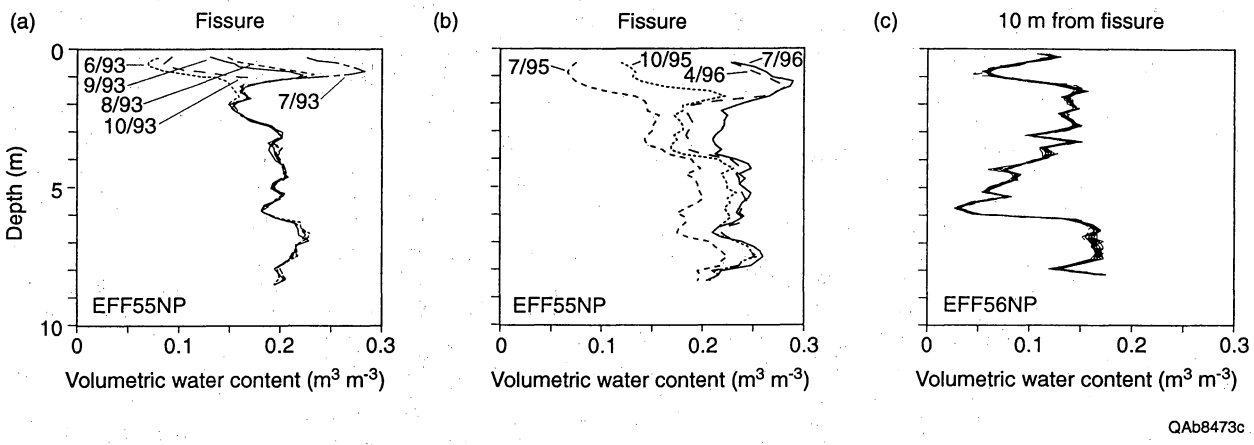
(a)
Fissure
(b)
Fissure
(c)
10 m from fissure
Depth (m)
0
5
10
6/93
9/93
8/93
10/93
7/93
7/95
10/95
4/96
7/96
EFF55NP
EFF55NP
EFF56NP
0
0.1
0.2
0.3
Volumetric water content (m3 m-3)
Volumetric water content (m3 m-3)
Volumetric water content (m3 m-3)

QAb8473c

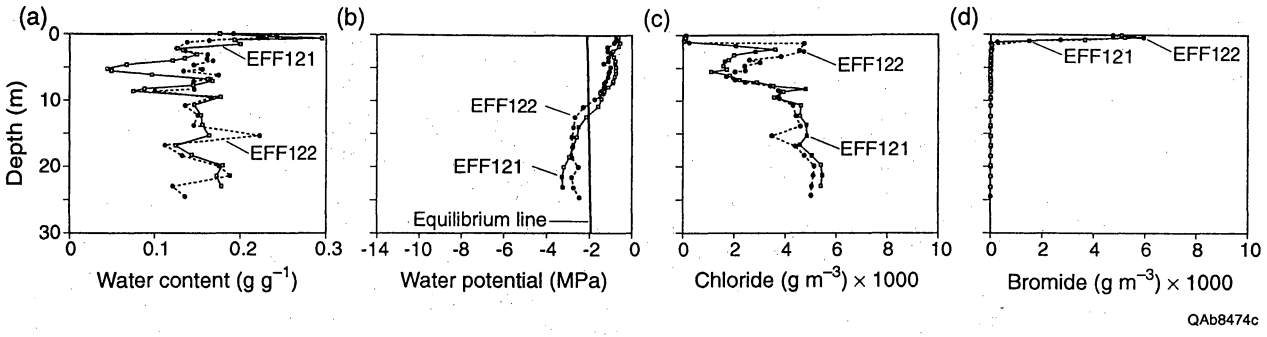
(a)
(b)
(c)
(d)
Depth (m)
0
10
20
30
EFF121
EFF122
0
0.1
0.2
0.3
Water content (g g^{-1})
EFF122
EFF121
Equilibrium line
-14
-10
-8
-6
-4
-2
0
Water potential (MPa)
EFF122
EFF121
0
2
4
6
8
10
Chloride (g m^{-3}) × 1000
EFF121
EFF122
0
2
4
6
8
10
Bromide (g m^{-3}) × 1000
QAb8474c

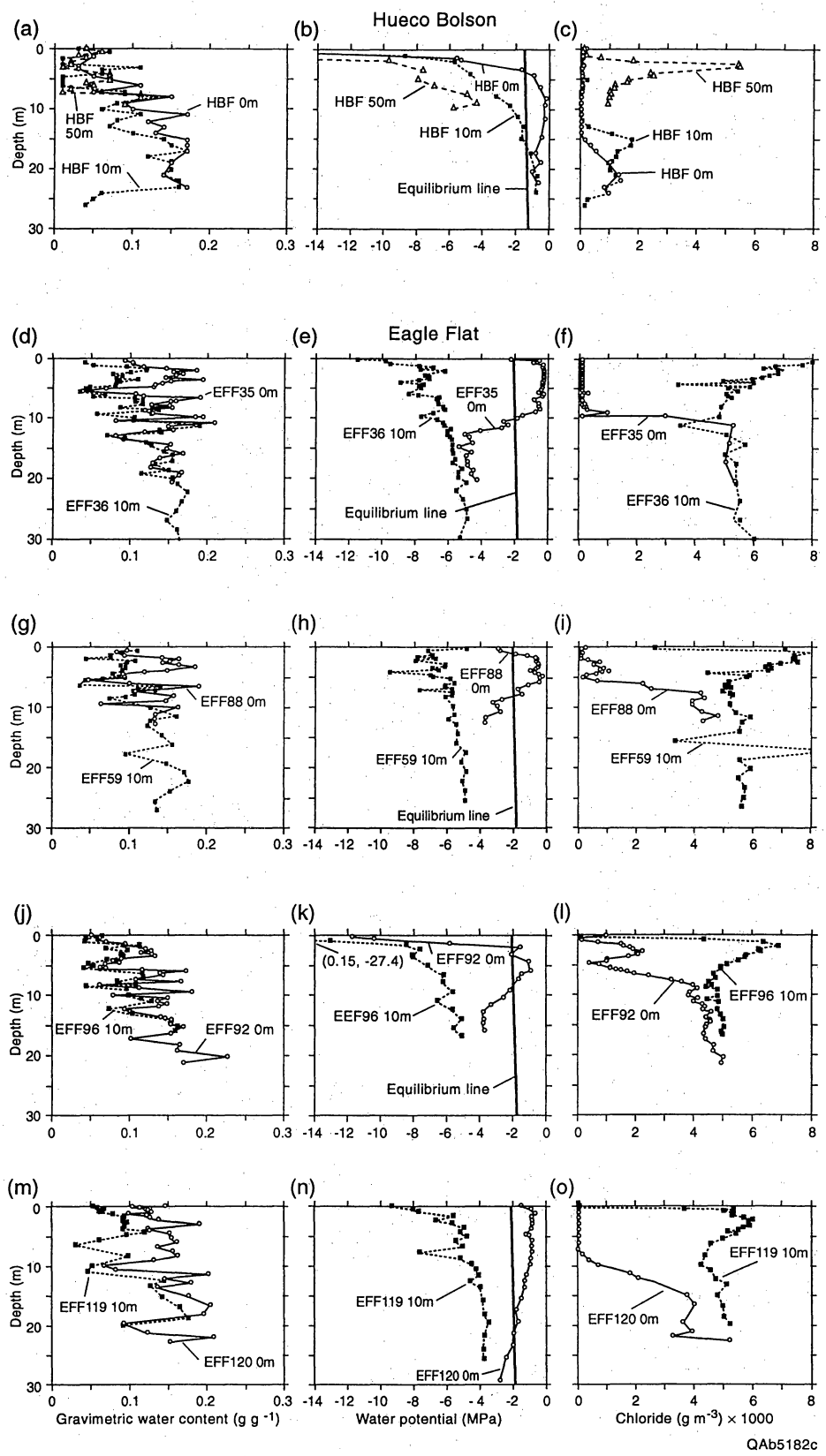
(a)
(b)
Hueco Bolson
(c)
HBF 0m
HBF 50m
HBF 10m
Equilibrium line
(d)
(e)
Eagle Flat
(f)
EFF35 0m
EFF36 10m
(g)
(h)
(i)
EFF88 0m
EFF59 10m
(j)
(k)
(l)
(0.15, -27.4)
EFF92 0m
EEF96 10m
EFF96 10m
(m)
(n)
(o)
EFF119 10m
EFF120 0m
Depth (m)
Gravimetric water content (g g -1)
Water potential (MPa)
Chloride (g m-3) × 1000
QAb5182c

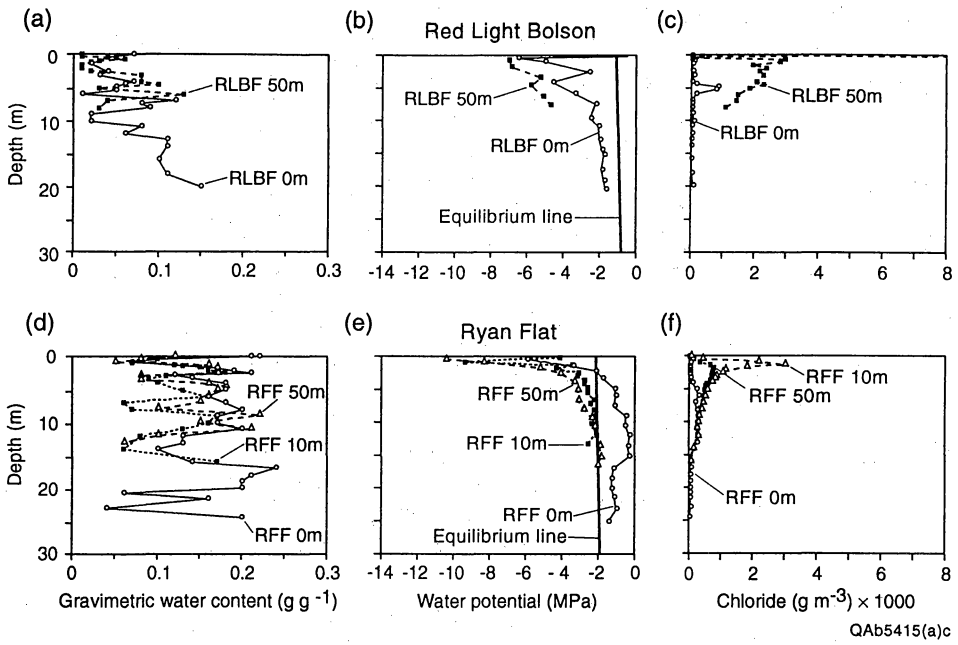
(a)
(b)
Red Light Bolson
(c)
Depth (m)
RLBF 50m
RLBF 0m
Equilibrium line
(d)
(e)
Ryan Flat
(f)
RFF 50m
RFF 10m
RFF 0m
Gravimetric water content (g g -1)
Water potential (MPa)
Chloride (g m-3) x 1000
QAb5415(a)c

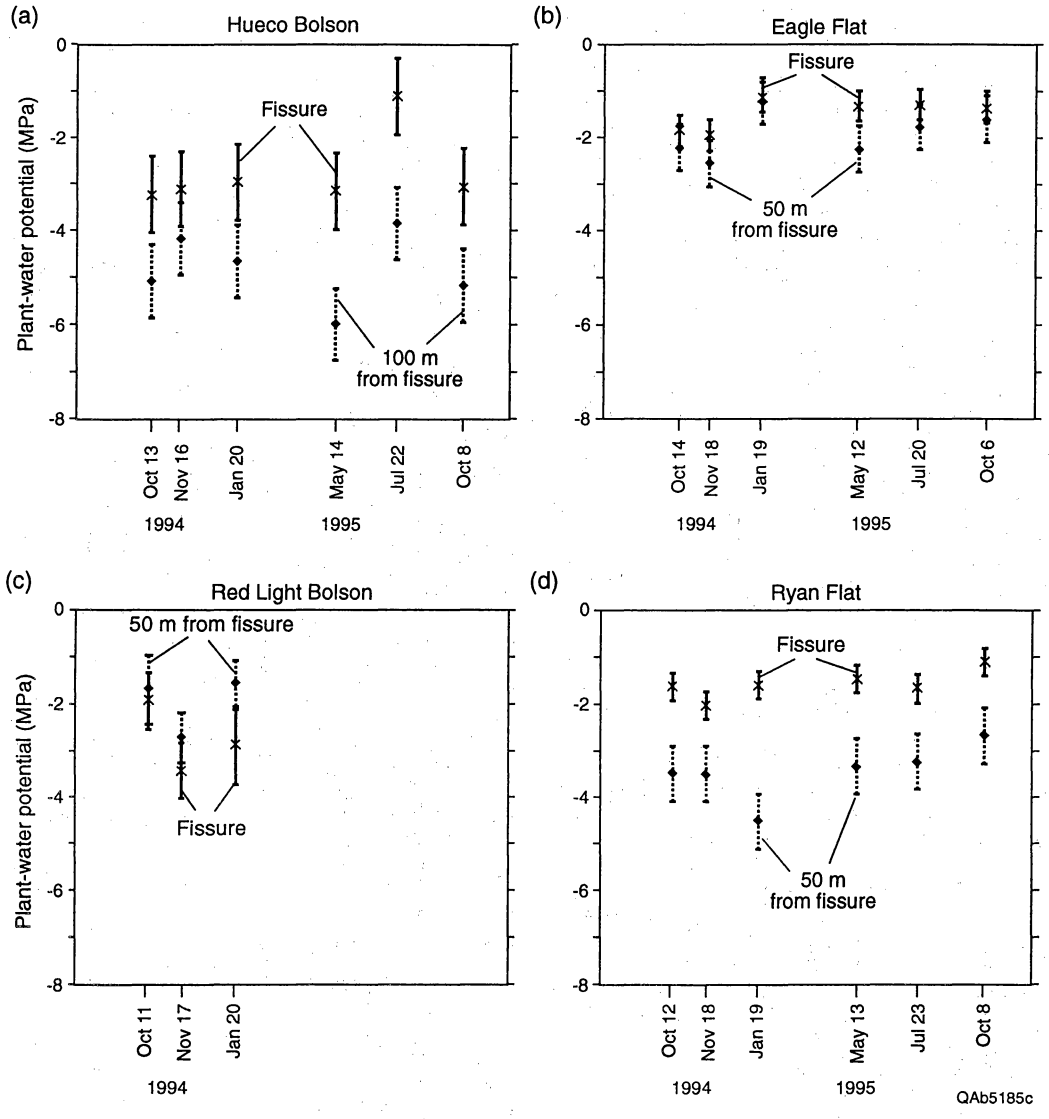
(a)
Hueco Bolson
Plant-water potential (MPa)
0
-2
-4
-6
-8
Fissure
100 m
from fissure
Oct 13
Nov 16
Jan 20
May 14
Jul 22
Oct 8
1994
1995
(b)
Eagle Flat
Fissure
50 m
from fissure
Oct 14
Nov 18
Jan 19
May 12
Jul 20
Oct 6
1994
1995
(c)
Red Light Bolson
50 m from fissure
Fissure
Oct 11
Nov 17
Jan 20
1994
(d)
Ryan Flat
Fissure
50 m
from fissure
Oct 12
Nov 18
Jan 19
May 13
Jul 23
Oct 8
1994
1995
QAb5185c

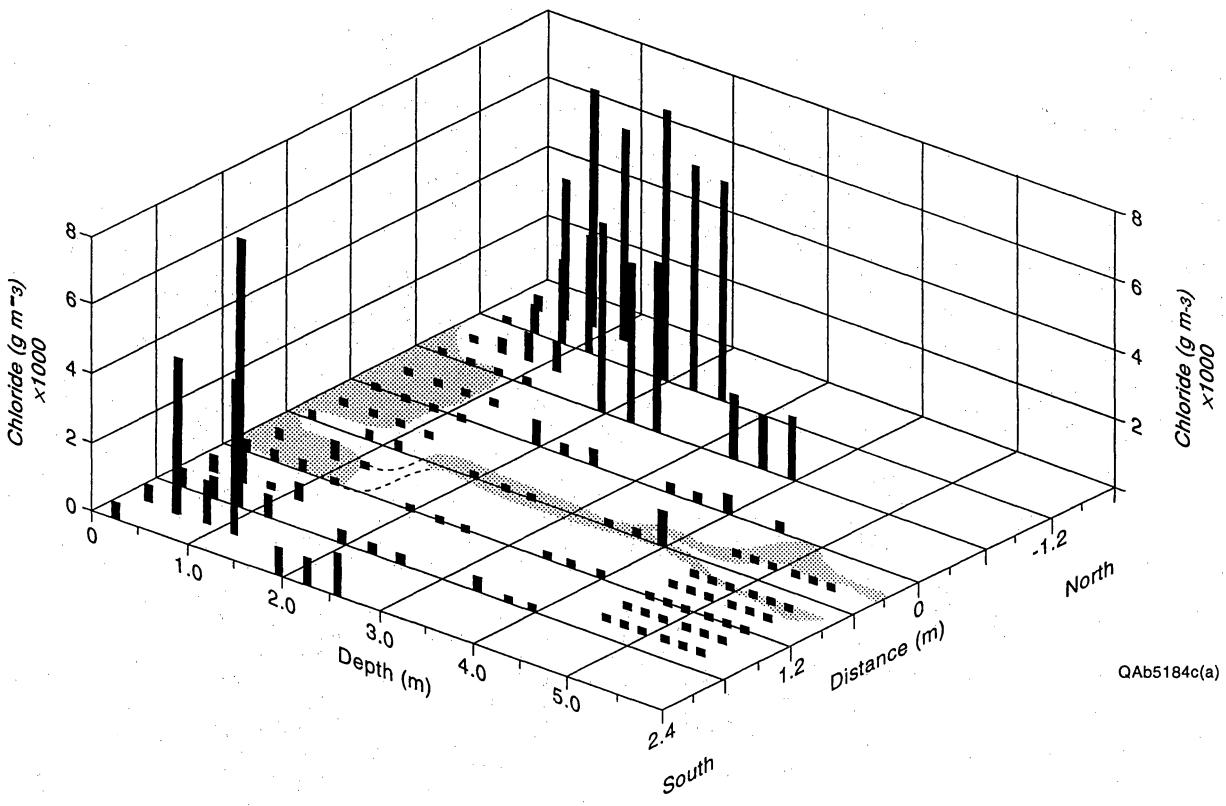

Eagle Flat fissure

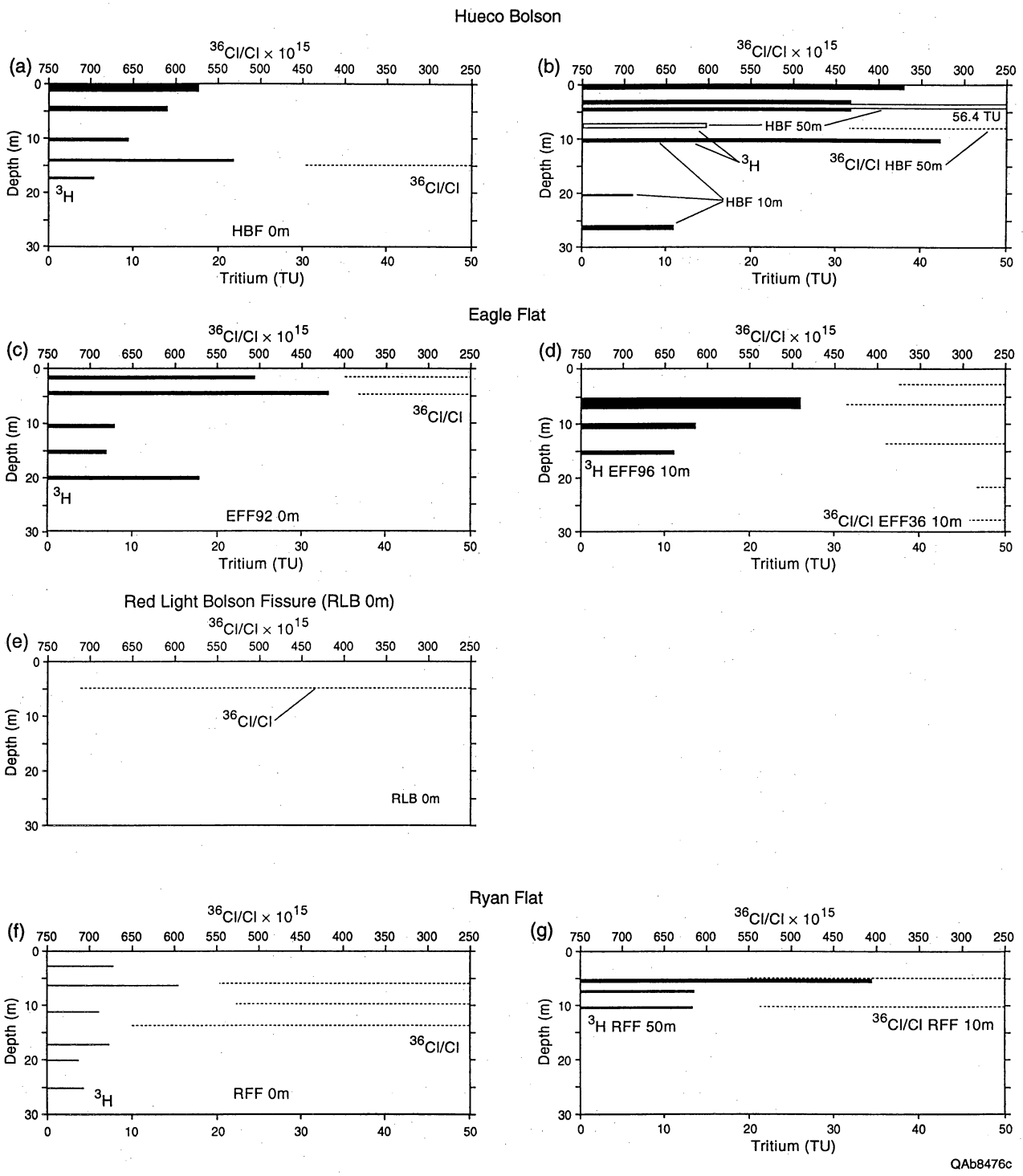
Hueco Bolson
(a)
(b)
^{36}Cl/Cl × 10^{15}
Depth (m)
Tritium (TU)
^{3}H
^{36}Cl/Cl
HBF 0m
HBF 50m
56.4 TU
HBF 10m
^{36}Cl/Cl HBF 50m
Eagle Flat
(c)
(d)
EFF92 0m
^{3}H EFF96 10m
^{36}Cl/Cl EFF36 10m
Red Light Bolson Fissure (RLB 0m)
(e)
RLB 0m
Ryan Flat
(f)
(g)
RFF 0m
^{3}H RFF 50m
^{36}Cl/Cl RFF 10m
QAb8476c

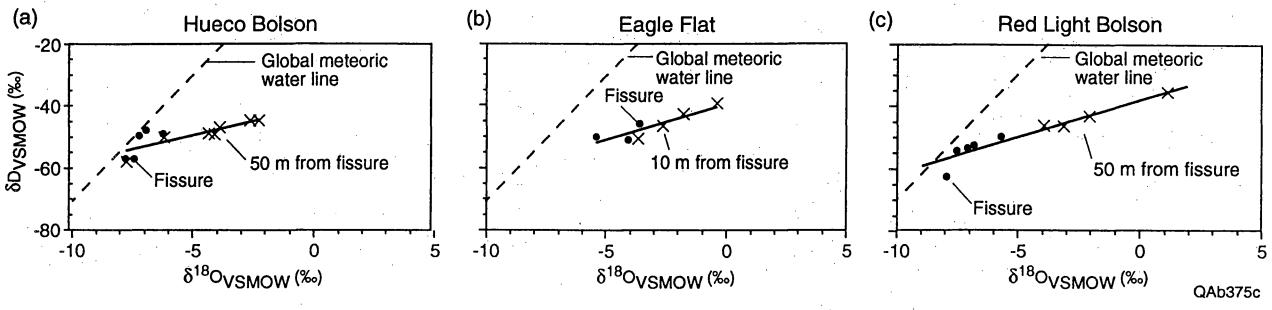
(a)
Hueco Bolson
Global meteoric water line
50 m from fissure
Fissure
δDVSMOW (‰)
δ18OVSMOW (‰)
-20
-40
-60
-80
-10
-5
0
5
(b)
Eagle Flat
Global meteoric water line
Fissure
10 m from fissure
(c)
Red Light Bolson
Global meteoric water line
50 m from fissure
Fissure
QAb375c

(a)

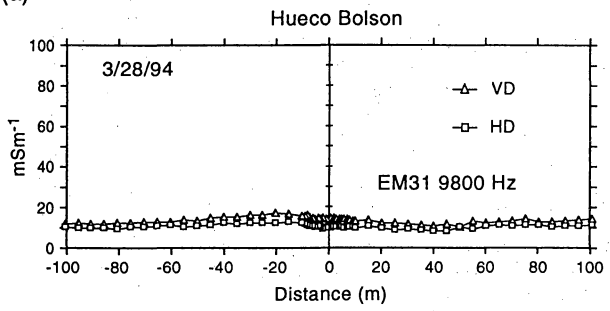

(b)

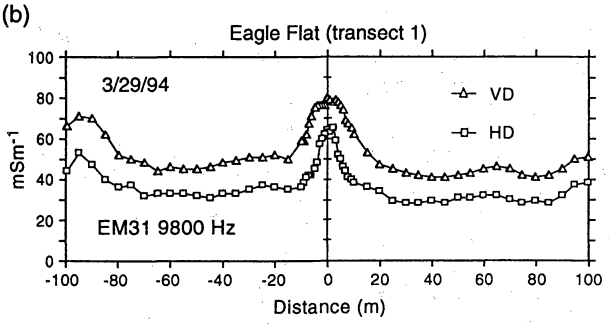

(c)

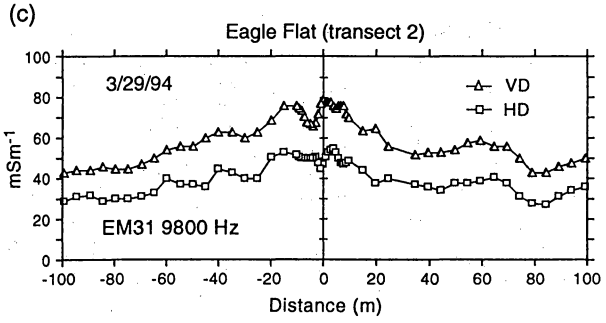

(d)

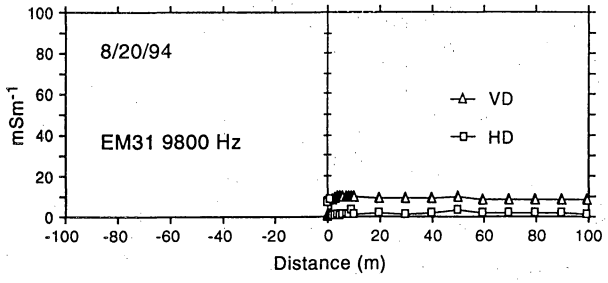

(e)

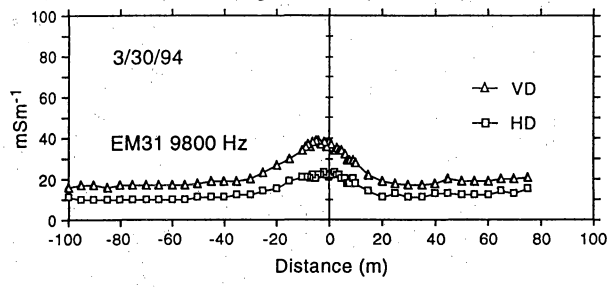

(f)

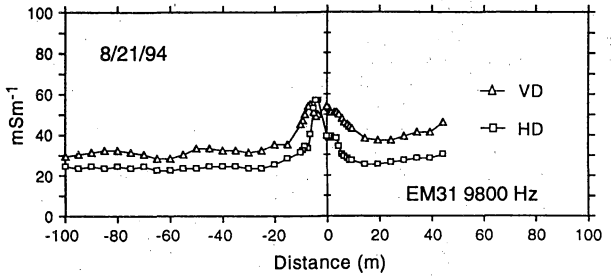

(g)

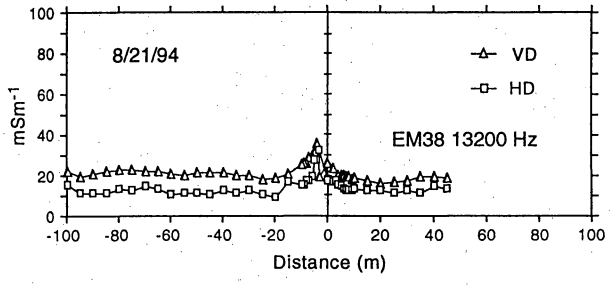

QAb349c

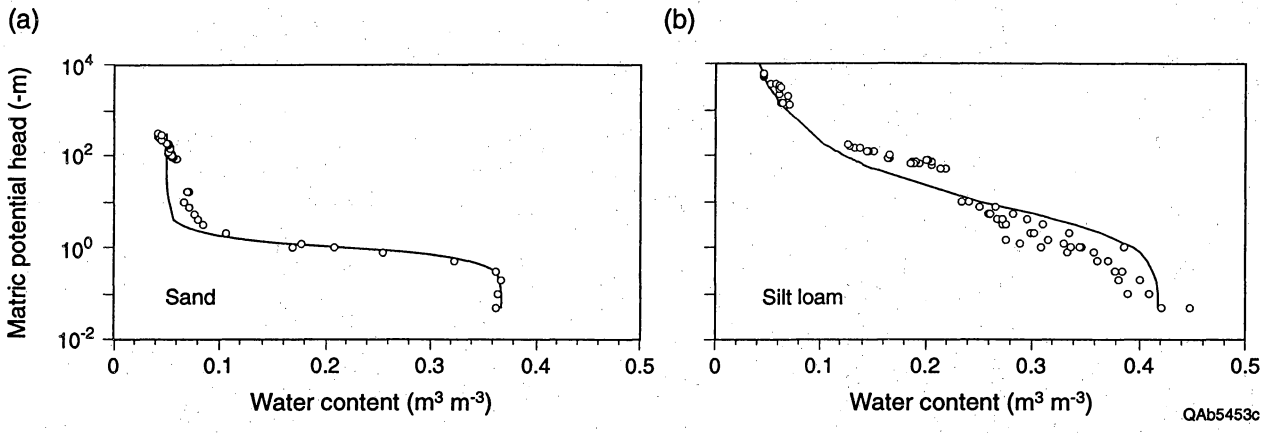
(a)
(b)
Matric potential head (-m)
10^4
10^2
10^0
10^{-2}
Sand
Silt loam
0
0.1
0.2
0.3
0.4
0.5
Water content (m^3 m^{-3})
Water content (m^3 m^{-3})
QAb5453c